INTERACTION NOTES

NOTE 198

THE ANALYSIS OF MONOPOLE ANTENNAS LOCATED ON A SPHERICAL VEHICLE†

OCTOBER 1974

F. M. Tesche*
A. R. Neureuther**
R. E. Stovall**

ABSTRACT

In this paper, a technique for determining the behavior of thin-wire antennas mounted radially on a conducting sphere is formulated and verified numerically and experimentally. The analysis method for this problem involves the formulation and solution of an integral equation for the antenna current. By a proper choice of the boundary condition at the sphere surface, which the Green's tensor for the problem satisfies, the range of integral equation is limited to over the wires only. The effect of the sphere is included in the Green's tensor. Numerical results for a number of different structures are presented.

---

† Portions of the formulation of this problem have been discussed in IN 137.

* with Science Applications, Inc., Berkeley, California 94701.

** with the Department of Electrical Engineering and Computer Science, University of California, Berkeley 94720.

I. INTRODUCTION

One problem which constantly arises in electromagnetic compatibility analysis of satellites, aircraft and other vehicles is that of assessing the degree of mutual interaction between two or more antennas which are located on the vehicle. A particular antenna may have a certain input impedance and radiation pattern when located on a vehicle. If additional antennas or other conducting elements are connected to the vehicle, the properties of the original antenna can be significantly different.

Not only do additional antennas affect the overall antenna behavior, but the size and shape of the vehicle itself are important. By being able to analyze such problems, it may be possible to locate various antennas on a particular vehicle so as to minimize the electromagnetic coupling and interference between them. Moreover, the radiation pattern of a specific antenna will depend on its location with respect to the other antennas. By locating an antenna correctly on a vehicle, interference from sources in a particular direction can be reduced.

Such radiation problems can, in principle, be treated by a variety of numerical methods. The most general method is to formulate an integral equation for the unknown surface currents flowing on both the vehicle and on the antennas. The solution for the current is then found by using the method of moments[4] to obtain a system of linear equations from the integral equation. This system of equations is then solved numerically on the computer. This method can be used for obstacles of arbitrary shape and for any number of antennas on the obstacle.

In practice, however, this method is severely limited due to computer time and storage requirements. Only relatively simple geometries have been treated and their sizes are usually small compared to a wavelength. A possible way around these difficulties is to employ a modified kernel in the integral equation which serves to reduce the range of the equation from over the entire structure to only over the antennas.

The idea of using a modified Green's function for formulating integral equations is well established. Aside from the discussions of

this method in various texts[7,8,17], other investigators have explored the use of this method. Kammler[10] has investigated the static charge distributions on circular cylinders within a parallel plate region, Rao[14], Taylor[18] and Tesche[20] have considered the radiating properties of antennas within parallel plates. Similarly, this method has been utilized for the analysis of periodic structures by others[9,15]. It appears, however, that this technique has not been widely applied numerically to problems involving antennas which are exterior to a conducting obstacle.

This paper considers the behavior of a number of monopole antennas radially oriented on a perfect conducting sphere using the modified Green's function approach. A spherical obstacle was chosen since the form of the modified Green's function is well known. In addition, the numerical results to be presented will be useful for applications to satellites (which may take on roughly spherical shape) having monopole antennas or sensor booms.

Even for certain vehicle shapes which are not coincident with a constant coordinate surface, and thereby admitting an eigenfunction expansion for the Green's function, this method can be used. The Green's function can be computed numerically beforehand as described by Harrington[5]. This computation necessitates actually solving the surface integral equation for the vehicle currents, once for each orientation and position of a unit current element.

II. FORMULATION OF THE INTEGRAL EQUATION

Consider the electromagnetic radiation or scattering from a conducting sphere of radius a with i radially directed wires of length L_i and radius b_i at various angles (θ_i,ϕ_i), as shown in Figure 1. The scattered electric field, $\bar{E}^{sca}$, produced by the currents on the wires and by the sphere surface currents (both of which are excited either by an incident plane wave for the scattering problem or by driving sources at the junctions of the wires and sphere for the antenna problem) may be written as

$$\bar{E}^{sca}(\bar{r}_o) = j\omega\mu \int_{\substack{\text{sphere} \\ \& \text{ wires}}} \bar{J}(\bar{r}_s)\cdot\underset{\sim}{\Gamma}_{fs}(\bar{r}_s,\bar{r}_o)ds \quad , \qquad (1)$$

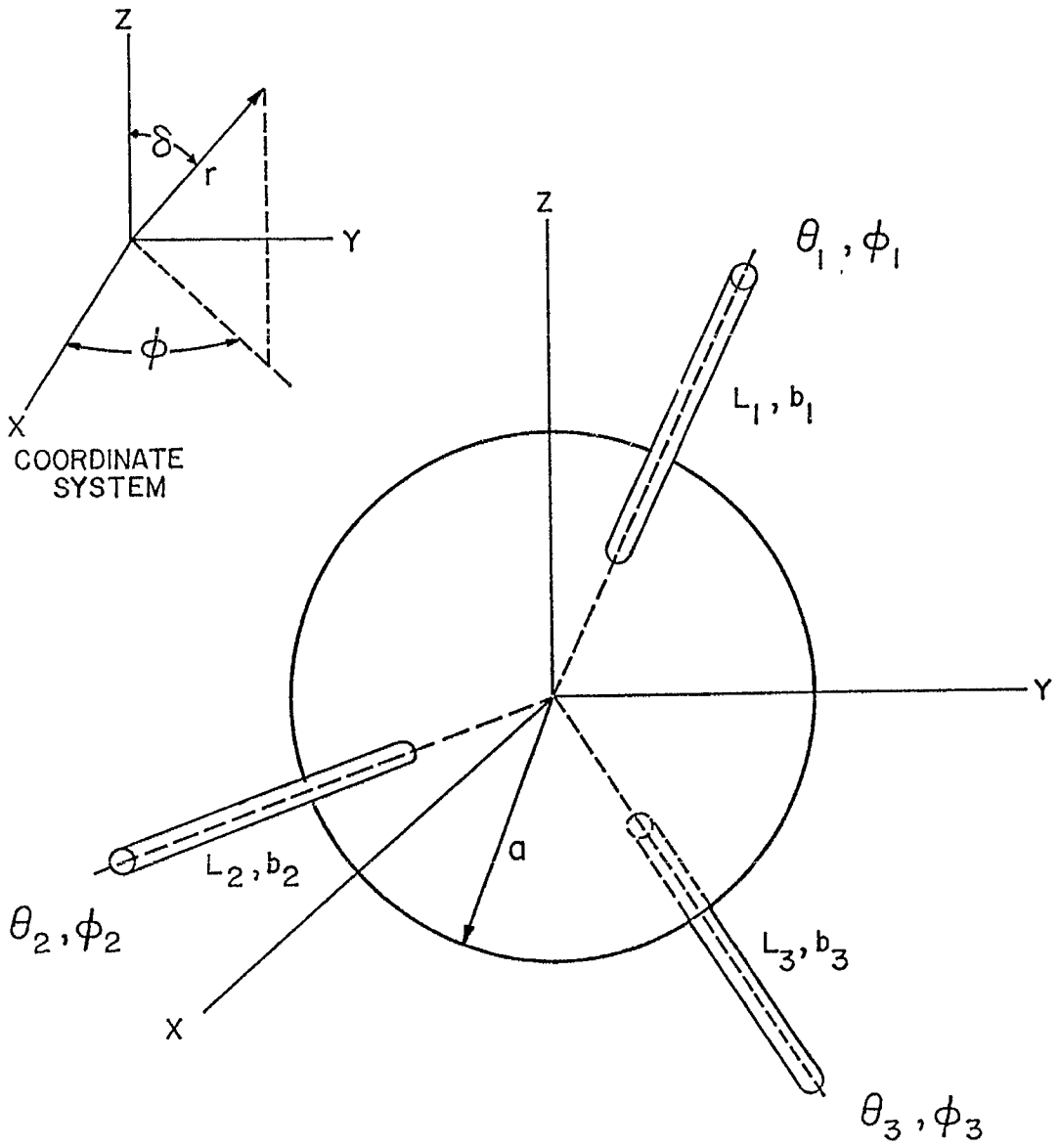

Figure 1. Geometry of the problem.

where $\underset{\sim}{\Gamma}_{fs}$ is the free space electric field Green's tensor as described by Tai[17]. If, however, one uses the Green's tensor which satisfies

$$\hat{n}_s \times \underset{\sim}{\Gamma}(\bar{r}_s, \bar{r}_o) = 0 \qquad (2)$$

for r_s on the sphere surface, it is possible to show that the integral in Eq. (1) extends only over the wires. Thus, it is necessary to determine only the wire currents to solve the problem.

For the geometry under consideration, only radially directed currents flow on the thin wires. Moreover, the component of the electric field needed to form the integral equation for the wire current is only the radial component. Noting that for the perfectly conducting wire, $E_r^{inc} + E_r^{sca} = 0$ on the wire surfaces, Eq. (1) yields the following integral equation for the wire currents:

$$-E_r^{inc}(\bar{r}_o) = j\omega\mu \int_{wires} J_r(\bar{r}_s)\, \Gamma_{rr}(\bar{r}_s, \bar{r}_o)\, ds \quad . \qquad (3)$$

As in all thin-wire problems, only the total current flowing in the wire is computed.

The (rr) component of the spherical Green's tensor is derived by Jones[8] and has the form

$$\Gamma_{rr}(\bar{r}_o, \bar{r}_s) = \sum_{n=1}^{\infty} \frac{n(n+1)(2n+1)}{r_o\, r_s} \Big[j_n(kr_<) h_n^{(2)}(kr_>) + T_n h_n^{(2)}(kr_o) h_n^{(2)}(kr_s) \Big] P_n(\cos\gamma) \qquad (4)$$

where $r_{(\lessgtr)}$ represents the $\begin{pmatrix}\text{smaller}\\ \text{larger}\end{pmatrix}$ of r_o and r_s, and j_n and $h_n^{(2)}$ represent the spherical Bessel and Hankel functions respectively. The angle γ is that between the two vectors $\bar{r}_o$ and $\bar{r}_s$ as shown in Figure 2. The factor T_n takes into account the presence of the sphere and has the values

$$T_n = -\frac{\frac{d}{da} a j_n(ka)}{\frac{d}{da} a h_n(ka)} \qquad (5)$$

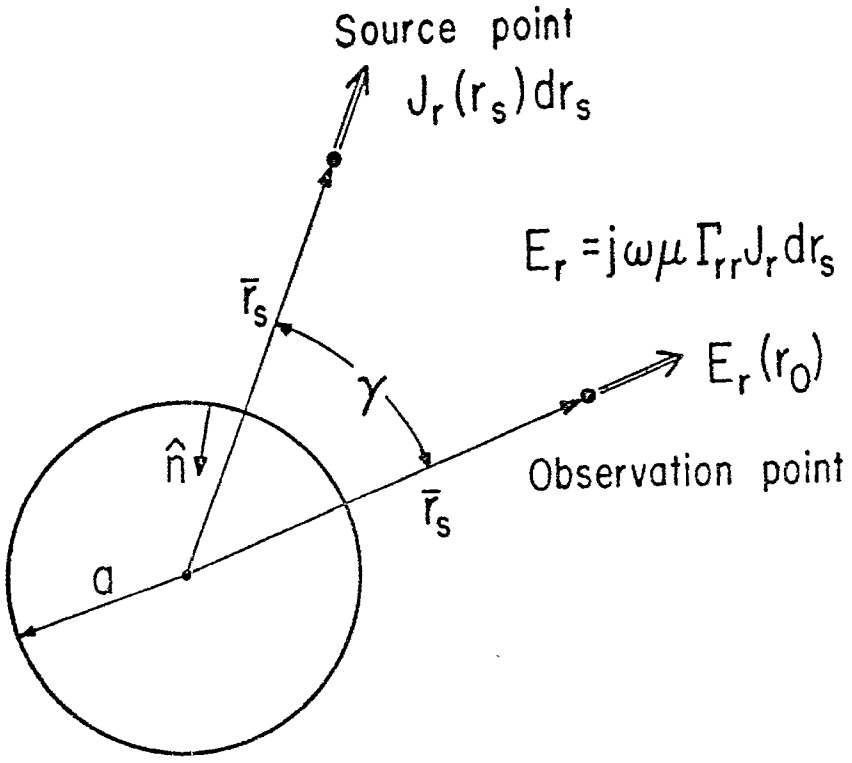

Figure 2. General locations of the source and observation points in the presence of the sphere.

for a perfectly conducting sphere of radius a. For a sphere of finite conducting material, this term may be modified as outlined in Jones.

The integral equation, Eq. (3), for the current on the antenna looks similar to the integro-differential equation of the Pocklington type for a single isolated scatterer or antenna[20]. This type of equation is written as

$$-E_r^{inc}(r_o) = \frac{1}{j\omega\varepsilon}\left(\frac{d^2}{dr_o^2} + k^2\right) \int_{wire} J_r(\bar{r}_s)\frac{e^{-jk|\bar{r}_o-\bar{r}_s|}}{4\pi|\bar{r}_o-\bar{r}_s|}\,ds \quad , \qquad (6)$$

and is known to have a triplet-type singularity in the kernel as $r_o \to r_s$ if the indicated derivatives are carried out explicitly. This necessitates the use of the finite difference technique in order to determine a solution[4]. By analogy it is expected that the infinite sum in Eq. (4) will contain a similar triplet singularity as $r_o \to r_s$, so it is desirable to rewrite Eq. (3) as an integro-differential equation, as was done in the isolated dipole case.

If $g_n(kr)$ represents any spherical Bessel function, then by definition[1]

$$\frac{d^2g_n}{dr^2} + \frac{2}{r}\frac{dg_n}{dr} + \left[k^2 - \frac{n(n+1)}{r^2}\right] g_n = 0 \quad . \qquad (7)$$

Defining the function $f_n(kr) = krg_n(kr)$ and taking the appropriate derivatives, it is found from Eq. (7) that

$$\left[\left(\frac{d^2}{dr^2} + k^2\right) - \frac{n(n+1)}{r^2}\right] f_n(kr) = 0 \qquad (8)$$

or equivalently,

$$\frac{n(n+1)g_n(kr)}{r} = \left(\frac{d^2}{dr^2} + k^2\right) rg_n(kr) \quad . \qquad (9)$$

Substituting into Eqs. (3) and (4), an equation of the Pocklington form results:

$$-E_r^{inc}(\bar{r}_o) = j\omega\mu\left(\frac{d^2}{dr_o^2} + k^2\right)\int_{wires} J_r(\bar{r}_s)K(\bar{r}_s,\bar{r}_o)ds \qquad (10)$$

where the kernel $K(\bar{r}_s,\bar{r}_o)$ is given by

$$K(\bar{r}_s,\bar{r}_o) = \frac{j}{4\pi k}\sum_{n=1}^{\infty}\frac{r_o}{r_s}(2n+1)\left[j_n(kr_<)h_n^{(2)}(kr_>)\right.$$

$$\left. + T_n h_n^{(2)}(kr_o)h_n^{(2)}(kr_s)\right]P_n(\cos\gamma) \quad . \qquad (11)$$

In solving Eq. (10), it is necessary to evaluate the kernel K in an efficient manner. If the calculation of K requires more time than to solve the equivalent set of coupled integral equations using the simpler free space Green's tensor, this method will not be a useful one. From the isolated thin-wire problem, it is known that the kernel in Eq. (6) has a singularity of the form $|r_o-r_s|^{-1}$. If there is a similar singularity in the kernel of Eq. (11), it is expected that the series would converge very slowly at points near $r_o \approx r_s$ and, in fact, diverge when $r_o = r_s$. Thus, it would be advantageous to put Eq. (11) in closed form for rapid numerical computation.

In investigating Eq. (11), it is seen that there are two terms in the summation. The first term involving j_n and $h_n^{(2)}$ represents the direct contribution of the source on the observed electric field, while the second term, involving factor T_n, represents the effect of the sphere on the observed field. The singularity in the kernel will occur in the first term as $\bar{r}_o \to \bar{r}_s$.

The addition theorem for spherical Hankel function[5] will permit the summation of the first part of the kernel K. It may be shown that

$$h_o^{(2)}\left(|r_o-r_s|\right) = \sum_{n=0}^{\infty}(2n+1)j_n(r_<)h_n^{(2)}(r_>)P_n(\cos\gamma) \qquad (12)$$

and that

$$h_o^{(2)}(R) = j\,\frac{e^{-jR}}{R} \qquad (13)$$

Thus, upon noting that Eq. (12) is essentially the first part of Eq. (11), aside from the $n = 0$ term, it is possible to express the kernel K as:

$$K(\bar{r}_s,\bar{r}_o) = \frac{j}{4\pi k}\frac{r_o}{r_s}\left[\frac{je^{-jk|\bar{r}_o-\bar{r}_s|}}{k|\bar{r}_o-\bar{r}_s|} - j_o(kr_<)h_o^{(2)}(kr_>) + \sum_{n=1}^{\infty} T_n(2n+1)h_n^{(2)}(kr_s)h_n^{(2)}(kr_o)P_n(\cos\gamma)\right] . \quad (14)$$

Hence, the first portion of the kernel, which is singular at $\bar{r}_o = \bar{r}_s$, may be summed in closed form, leaving only the reflection contribution to be summed numerically. This kernel as given by Eq. (14) and the relation in Eq. (10) describes the Pocklington integro-differential equation for the currents flowing on the wire in the presence of the sphere.

It should be pointed out that, for the case of a single wire on the sphere, the angle γ between the source point $(\bar{r}_s)$ and the observation point $(\bar{r}_o)$ is zero, thereby causing the $P_n(\cos\gamma)$ term to be unity for all values of n. For the more general case where there are other wires on sphere, this term needs to be included.

The solution of Eq. (10) is often facilitated by assuming that the surface current J on the antenna wire can be replaced by the same amount of total current $I = 2\pi bJ$ which flows along the axis of the wire. The factor b is the radius of the wire. With this thin-wire approximation, the factor $|\bar{r}_o-\bar{r}_s|$ in Eq. (14) is never singular. Care must be exercised in using this approximation, however, as is discussed in Ref. (21).

In the derivation of the Pocklington equation, it was assumed that both the current $\bar{J}$ and the incident electric field $\bar{E}_{inc}$ were in the radial direction only and therefore related simply by the Green's tensor component Γ_{rr}. In the limiting case of a very thin cylindrical dipole mounted on a relatively large sphere this is a good approximation, but it is never exact due to the finite thickness of the wire. Therefore, if a more exact solution is desired for thicker wires, both the $\hat{\theta}$ and $\hat{r}$ components of $\bar{E}$ and $\bar{J}$ must be considered and suitably related through the four components of the Green's tensor, Γ_{rr}, $\Gamma_{r\theta}$, $\Gamma_{\theta r}$ and $\Gamma_{\theta\theta}$.

III. DETERMINATION OF THE INCIDENT FIELD: SCATTERING PROBLEM

The source term for the Pocklington equation depends on the tangential component of the electric field incident on the wires due to a driving source on the wire itself (antenna problem) or due to an incident plane wave (scattering problem). Note that in evaluating this tangential field, the presence of the conducting sphere must be accounted for. In the scattering problem, the field incident on the wire consists of two parts, as shown in Figure 3. One is a direct contribution of the incident field and the other is a reflection from the spherical obstacle.

The scattering of an incident field by a conducting sphere is presented in detail by Harrington[6]. For a scattering problem where the incident plane wave of magnitude E_o is $\hat{x}$ polarized and propagates in the $\hat{z}$ direction, the radial component of the electric field observed at point $\bar{r}_o = (r_o, \theta, \phi)$ is given by

$$E_r(\bar{r}_o) = \frac{1}{j\omega\varepsilon}\left(\frac{d^2}{dr_o^2} + k^2\right) A_r(\bar{r}_o) \quad . \tag{15}$$

The quantity A_r is the radially directed magnetic vector potential which generates field TM with respect to the $\hat{r}$ direction. This may be expressed in series form as shown by Harrington as

$$A_r(\bar{r}_i) = \frac{E_o}{\omega\mu}\cos\phi \sum_{n=0}^{\infty} kr_o \left[a_n j_n(kr_o) + b_n h_n^{(2)}(kr_o)\right] P_n^1(\cos\theta) \tag{16}$$

where

$$a_n = \frac{j^{-n}(2n+1)}{n(n+1)} \tag{17}$$

and

$$b_n = a_n T_n \tag{18}$$

where T_n is defined by Eq. (5). Using the relation in Eq. (8), the expression for the field in Eq. (15) can be simplified to yield

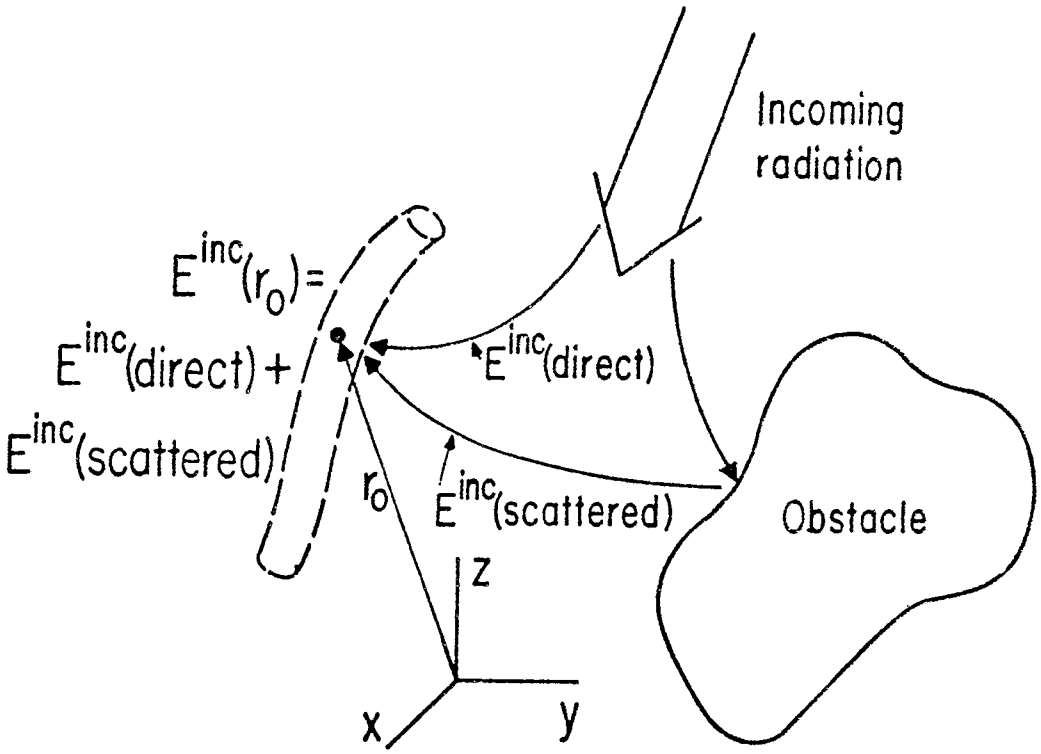

Figure 3. Total incident field on arbitrary wire antenna in presence of arbitrary obstacle.

$$E_r^{inc}(\bar{r}_o) = \frac{E_o \cos\phi}{jk} \sum \frac{j^{-n}(2n+1)}{r_o} P_n^1(\cos\theta)\left[j_n(kr_o) + T_n h_n^{(2)}(kr_o)\right] \tag{19}$$

This relation may be used to evaluate the forcing term in Eq. (10). Since the field is not singular along the wire as is the kernel in Eq. (14), it is not necessary to separate out the singular term to sum it directly. The complete sum in Eq. (19) may be done numerically without difficulty.

IV. DETERMINATION OF THE INCIDENT FIELD: ANTENNA PROBLEM

At this point it is desirable to consider the exact form of the electric field incident on the wire for the case of a driven antenna. This actual source which produces the incident field may then be related to a small voltage source between the antenna and the sphere.

For the case of a driven monopole on the sphere, the antenna will be assumed to be fed by a co-axial line having TEM excitation. This is shown in Figure 4. From the equivalence principle, a mathematical surface can be drawn about the antenna wire and an equivalent source of $\hat{n}\times\bar{H} = \bar{J}$ placed on this surface, thereby allowing the removal of the antenna wire. The incident electric field tangent to the mathematical surface may then be calculated by considering the excited aperture in the sphere to be radiating without the wire present. Figure 5 shows the geometry for this problem.

The radially directed electric field for the source in this problem is readily determined from the Green's tensor $\underset{\sim}{\Gamma}$. From Jones[8], it may be shown that the radiated electric field produced by an impressed tangential electric field $\bar{E}_s$ on the surface of the sphere is given by

$$\bar{E}_{inc}(\bar{r}_o) = \int_{\substack{\text{sphere}\\ \text{surface}}} \left[\hat{n}\times\bar{E}(\bar{r}_s)\right]\cdot\left[\nabla_s\times\underset{\sim}{\Gamma}(\bar{r}_s,\bar{r}_o)\right] ds \tag{20}$$

where $\underset{\sim}{\Gamma}$ is the Green's function obeying Eq. (2).

The electric field on the surface of the sphere is assumed to be related to the voltage across the co-axial line by the relation

$$E_\tau = \frac{V_o}{\tau \ln(c/b)} \approx E_\theta \tag{21}$$

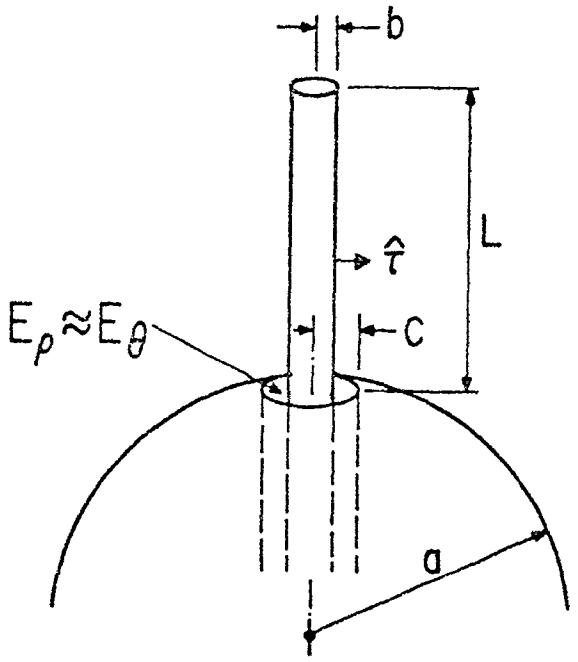

Figure 4. Assumed antenna feed.

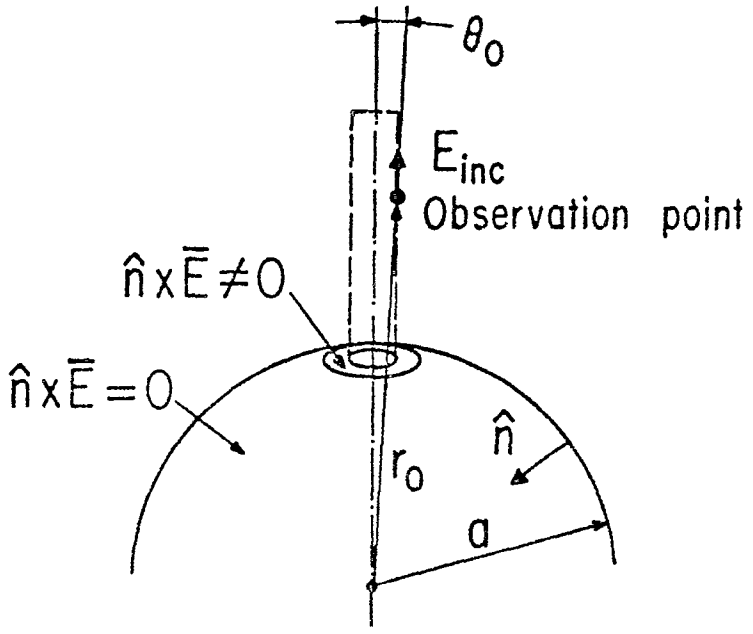

Figure 5. Geometry for computing incident electric field with antenna removed.

where τ is the radius of the cylindrical coordinate system for the co-axial line and b and c are the inner and outer radii of the line. Noting $\tau = a\sin\theta$, the impressed electric field is given by

$$E_\theta \approx \frac{V_o}{a\ \ln(c/b)\sin\theta} \quad . \tag{22}$$

for θ within the co-axial region and zero elsewhere.

Since $\hat{n}\times\bar{E}$ is in the $-\hat{\phi}$ direction and we wish to find E^{inc} in the $\hat{r}$ direction, it is desired to extract the $\hat{\phi}\hat{r}^{th}$ component of $\nabla_s \times \underset{\sim}{\Gamma}(\bar{r}_s, \bar{r}_o)$, which has the following form:

$$(\nabla\times\underset{\sim}{\Gamma})_{\phi r} = -\frac{ik}{4\pi}\sum_{n=1}^{\infty}\frac{2n+1}{r_o}\left[j_n(kr_<)h_n^{(2)}(kr_>) + T_n h_n(kr_o)h_n^{(2)}(kr_s)\right]$$

$$\times \frac{dP_n}{d\theta}(\cos\theta_o)P_n(\cos\theta_s) \tag{23}$$

where θ_o defines the observation point and θ_s defines the source point. Specializing this for $r_s \to a$ on the surface of a perfectly conducting sphere, and using the Wronskian to reduce the complexity of the Hankel functions, the following is obtained:

$$(\nabla\times\underset{\sim}{\Gamma})_{\phi r} = -\frac{k}{4\pi a r_o}\sum_{n=1}^{\infty}\frac{(2n+1)}{\frac{d}{da}\,a\,h_n(ka)}\,h_n^{(2)}(kr_o)P_n(\cos\theta_s)\,\frac{dP_n}{d\theta}(\cos\theta_o) \quad . \tag{24}$$

Substituting this and Eq. (22) into (20) yields:

$$E_r^{inc}(r_o) = \frac{V_o k}{2a^2\ \ln(c/b)}\int_{\theta_s=\sin^{-1}b/a}^{\theta=\sin^{-1}c/a}\sum_{n=1}^{\infty}\frac{2(n+1)}{\frac{d}{da}\left[ah_n(ka)\right]}\,\frac{h_n(kr_o)}{kr_o}$$

$$P_n(\cos\theta_o)\,\frac{\frac{dP_n}{d\theta}(\cos\theta_s)}{\sin\theta_s}\,(a^2\sin\theta_s d\theta_s) \tag{25}$$

where the integral over ϕ has already been carried out. Interchanging the order of the summation and using the following relationship,

$$\int_{\theta_1}^{\theta_2}\frac{dP_n}{d\theta}\,d\theta = P_n(X_2) - P_n(X_1) \tag{26}$$

where

$$X_2 = \cos\left[\sin^{-1}(c/a)\right]$$

and

$$X_1 = \cos\left[\sin^{-1}(b/a)\right] \quad ,$$

the resulting equation for the incident radial electric field is

$$E_r^{inc}(\bar{r}_o) = \frac{V_o k}{2\ \ln(c/b)} \sum_{n=1}^{\infty} \frac{2(n+1)}{\frac{d}{da}\, a h_n(ka)} \frac{h_n^{(2)}(kr_o)}{kr_o} P_n(\cos\theta_o)$$

$$\left[P_n(X_2) - P_n(X_1)\right] \quad . \tag{27}$$

This relation should be evaluated for observation points on the surface of the antenna wire and subsequently used in the integral equation to determine the current on the driven antenna.

V. THE RADIATED FIELDS AND THE SPHERE CURRENT

Once the currents on the monopole antennas are determined by a numerical solution of Eq. (10), the fields radiated by the currents on the entire structure can be found by evaluating Eq. (1) with only the $1/r_o$ terms in $\underset{\sim}{\Gamma}$ in Jones[8], it is observed that only the components of $\underset{\sim}{\Gamma}$ in the $\hat{\theta}$ and $\hat{\phi}$ directions exist in the far field. Moreover, for the special case of a radially directed current located at either polar axis of the sphere, only the $\hat{\theta}$ component of the radiated electric field is non-zero, and from the symmetry of the problem, is independent of the ϕ coordinate. This results in the fact that the $\Gamma_{r,\theta}$ component requires only one summation process instead of the two which are required in the most general case.

For a single monopole antenna located at $(0^o,0^o)$, the electric field can be expressed as

$$E_\theta(r_o,\theta) = j\omega\mu \int_{wire} I(r_s)\Gamma_{r\theta}(r_o,r_s)dr_s \tag{28}$$

with

$$\Gamma_{r,\theta} = -\frac{j}{4\pi k}\sum_{n=1}^{\infty}(2n+1)\,\frac{1}{r_o}\frac{d}{dr_o}\left[r_o h_n(k_o r)\right]\frac{dP_n}{d\theta}$$

$$\left[\frac{j_n(kr_s)}{r_s} - \frac{\frac{d}{da}aj_n(ka)}{\frac{d}{da}ah_n(ka)}\,\frac{h_n(kr_s)}{r_s}\right] \qquad (29)$$

and $I(r_s)$ being the numerically determined monopole current.

In looking at the far field components of Eq. (29), it is possible to replace the term $H_n(kr_o)$ by its asymptotic form

$$h_n(kr_o) \sim j^{(n+1)}\,\frac{e^{-jkr_o}}{kr_o} \qquad \text{as } r_o \to \infty \ . \qquad (30)$$

Similarly,

$$\frac{1}{r_o}\frac{d}{dr_o}\left[r_o h_n(kr_o)\right] \sim j^h\,k\,\frac{e^{-jkr_o}}{kr_o} \qquad \text{as } r_o \to \infty \ . \qquad (31)$$

With these simplifications, the radiated electric field is given by

$$E_\theta(r_o,\theta) = -\frac{Z_o k}{4\pi}\,\frac{e^{-jkr_o}}{kr_o}\int_{\text{wire}} I(r_s)\sum j^n\,\frac{(2n+1)}{r_s}\,P_n^1(\cos\theta)$$

$$\left[j_n(kr_s) - \frac{\frac{d}{da}aj_n(ka)}{\frac{d}{da}ah_n(ka)}\,h_n(ka)\right]dr_s \ . \qquad (32)$$

For more than one monopole located on the sphere, the radiated field is computed using a rotation of coordinates procedure as described by Du and Tai[3]. After the currents on all monopoles are computed, the contribution from each monopole to the total field is calculated by first rotating the antenna to the $(0^\circ,0^\circ)$ position, evaluating E_θ from Eq. (32), and then rotating the antenna back to its original position. In this manner, both E_θ and E_ϕ fields are produced, but it requires only the single summation process. Sample results for the sphere and two monopoles are presented in Ref. (19).

In a similar manner, the surface current density on the sphere can be computed. The magnetic field intensity at an observation point $\bar{x}$ exterior to the sphere is given by the following expression:

$$\bar{H}(\bar{r}_o) = -\frac{1}{j\omega\mu} \int_{\text{wires}} \nabla\times\underset{\sim}{\Gamma}(\bar{r}_o,\bar{r}_s)\cdot\bar{J}(\bar{r}_s)\, dv_s \quad . \quad (33)$$

By letting the observation point $\bar{r}_o$ approach the sphere, and noting that the tangential $\bar{H}$ field gives the induced surface currents, it is possible to obtain values for J_ϕ and J_θ on the sphere.

If there is only one radially directed monopole at $(0^\circ,0^\circ)$, the representation for $\nabla\times\underset{\sim}{\Gamma}$ becomes simpler, and it is seen that only a J_θ exists on the sphere. This is given by

$$J_\theta(\theta) = \int_{\text{wire}} I(r_s)\, K(a,\theta,r_s)\, dr_s \quad (34)$$

where the kernel K is

$$K(a,\theta,r_s) = -\frac{1}{4\pi a} \sum_{n=1}^{\infty} (2n+1)\, \frac{h_n(kr_s)}{r_s}\, \frac{P_n^1(\cos\theta)}{\frac{d}{da}\, a h_n(ka)} \quad . \quad (35)$$

For more than one monopole, the same rotational procedure used for the field calculation is employed to obtain values of J_θ and J_ϕ produced by each of the individual monopoles. The results are then superimposed so as to obtain the total surface currents.

VI. NUMERICAL RESULTS

The solution of the integral equation for the antenna currents was achieved by using the method of moments[4]. For this study, a pulse function expansion for the wire current was used, along with delta function testing. The driving source for the antenna was assumed to be the co-axial feed discussed in Section IV.

One important concern in carrying out a numerical solution to Eq. (10) is that the kernel of the integral equation be summed efficiently. It is well known that this type of series requires typically (ka) terms before the partial sum begins to converge. For extremely large spheres, the Watson transformation[23] has been developed to speed the convergence. For the present problem with sphere sizes on the order of two or three wavelengths, a direct summation of the terms is feasible. However, when the source and observation points lie near the sphere surface, the series becomes more and more slowly convergent. As a result, a nonlinear transformation of the partial sums of the slowly converging sequence, as described by Shanks[16], was employed to obtain the converged values of the kernel for the larger sphere sizes.

As a typical example, Figure 6 shows the converging behavior of the series in Eq. (14) for the case when the source points and the observation point lie along the $\theta = 0$ axis, and with the source point located on the sphere surface. Both the real and imaginary parts of the resulting sum are shown as a function of the number of terms, N.

After five terms, it is seen that for a sphere radius of $.25\lambda$, the real part of the series has converged for all of the different observation points. After sixty terms, however, the imaginary part of the series still has not converged for the observation point at $r_o = .27\lambda$. Let S_n denote the imaginary part of the sum after n terms are added. Using the first twenty terms of the sequence, i.e., S_1, $S_2 \ldots S_{20}$, the resulting sum of the series as determined by the transformation is 4% higher than the sum obtained by taking 70 terms, S_{70}. The actual value of the sum S_{20} is seen to be 20% lower than the S_{70} term, clearly indicating that the transformation applied to the first twenty partial sums gives a good indication of the final value for the sum.

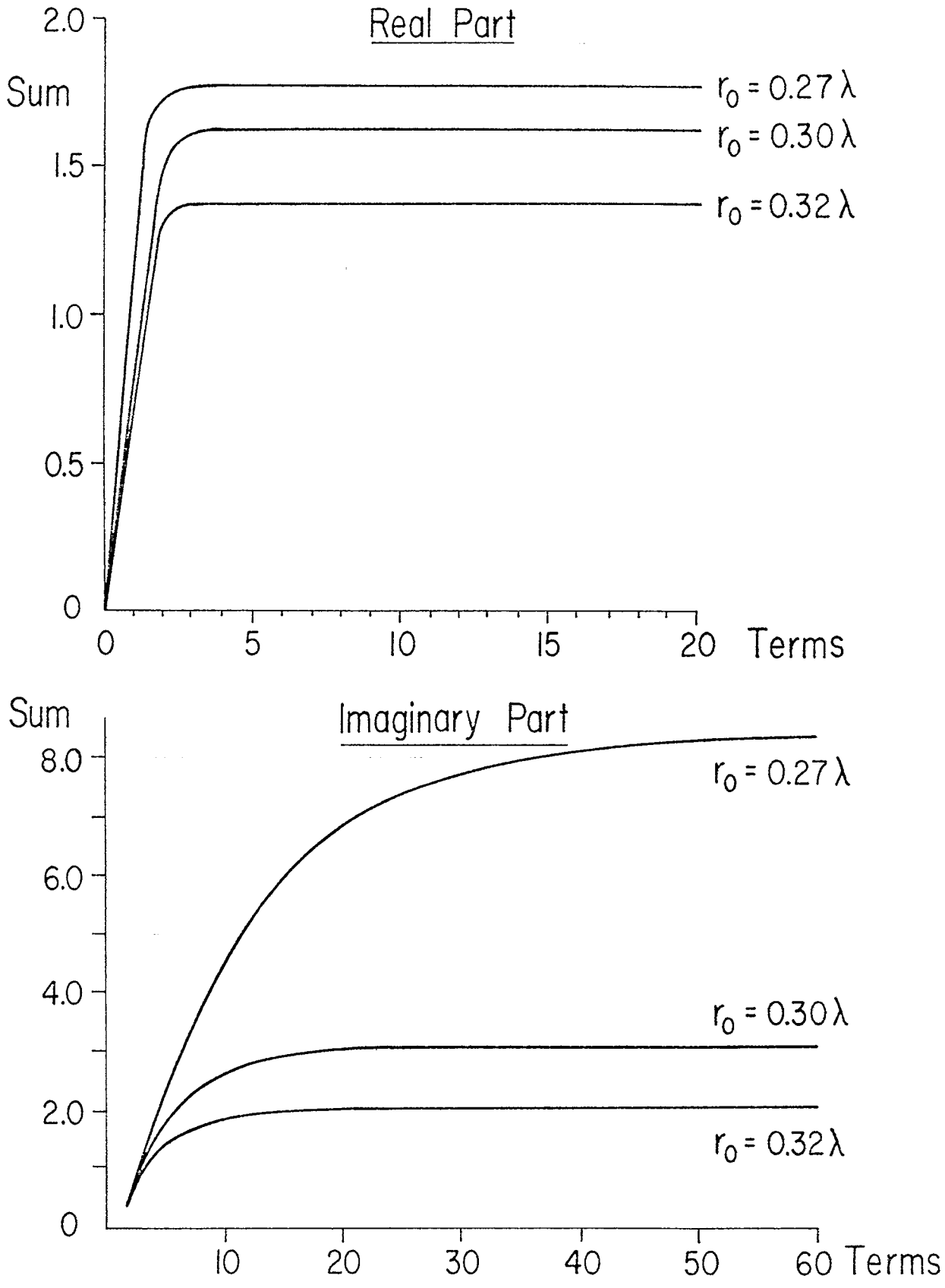

Figure 6. Partial sum of the kernel for $a = .25\lambda$, $\gamma = 0$, and $r_s = .25\lambda$.

If the sequence of partial sums S_{51}, $S_{52}...S_{60}$ are employed in the transformation, it is expected that the resulting value for the summation as given by the transformation will be more accurate due to the fact that the higher order partial sums themselves are more accurate. Comparing this value of the summation to that obtained by transforming the first twenty partial sums, it is seen that the difference is only .04%. Thus, the first twenty terms of this series can be used to adequately determine the final sum of this particular series.

A subroutine for carrying out this transformation was written and is employed to determine the resulting value of the kernel K if the number of terms in the series is insufficient to obtain adequate convergence. In the actual program, it was found that for a sphere radius of about .50λ and the specified error in the summation of Eq. (10) being .001, the nonlinear transformation was used for only about 10% of the kernel evaluations when 50 terms in the sum were used. For the determination of the current on a quarter wave monopole on a sphere of radius $a = .5\lambda$, and the subsequent calculation of the radiation pattern, the required computer time was approxiamtely three seconds on a CDC 6400. For this figure, seven zones on the structure were used.

As an example of typical results obtained from the calculations, Figure 7 shows the input impedance of a single monopole of length $L = .25\lambda$ and shape factor $\Omega = 2\ln(2L/b) = 10$, b being the wire radius, mounted on a sphere of variable radius. As the radius approaches a very large value, the monopole effectively sees an infinite ground plane instead of the sphere. The appropriate input impedance values for the ground plane, denoted by R and X are shown in the figure. It is interesting to note that even with a sphere of only 1λ in diameter, the input impedance is only about 10% high from that of the ground plane value.

Figure 8 shows the frequency domain response of the input impedance of a single monopole of length $L = a$ and $\Omega = 9.6$. This roughly compares with the size of the conical antenna treated by Bolle and Morganstern[2], and their results are shown by the dotted lines in the figure.

The radiation pattern of a single monopole of length $L = .25\lambda$ on a sphere of a variable radius from $a = .1\lambda$ to $.6\lambda$ is portrayed in Figure 9. Shown are normalized polar plots of the radiated power. Note

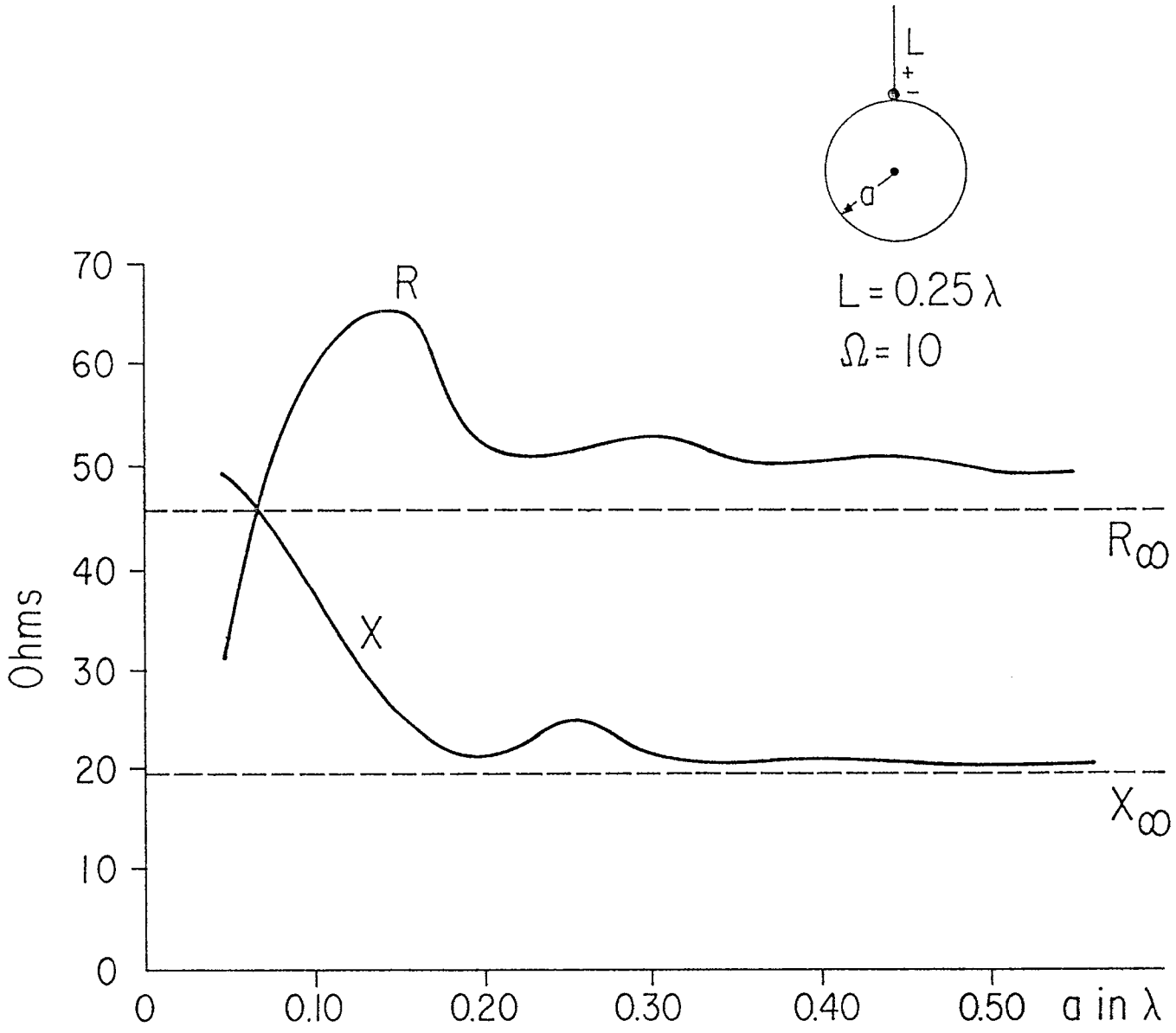

Figure 7. Input impedance R + jX of quarter wave monopole on sphere as function of sphere radius.

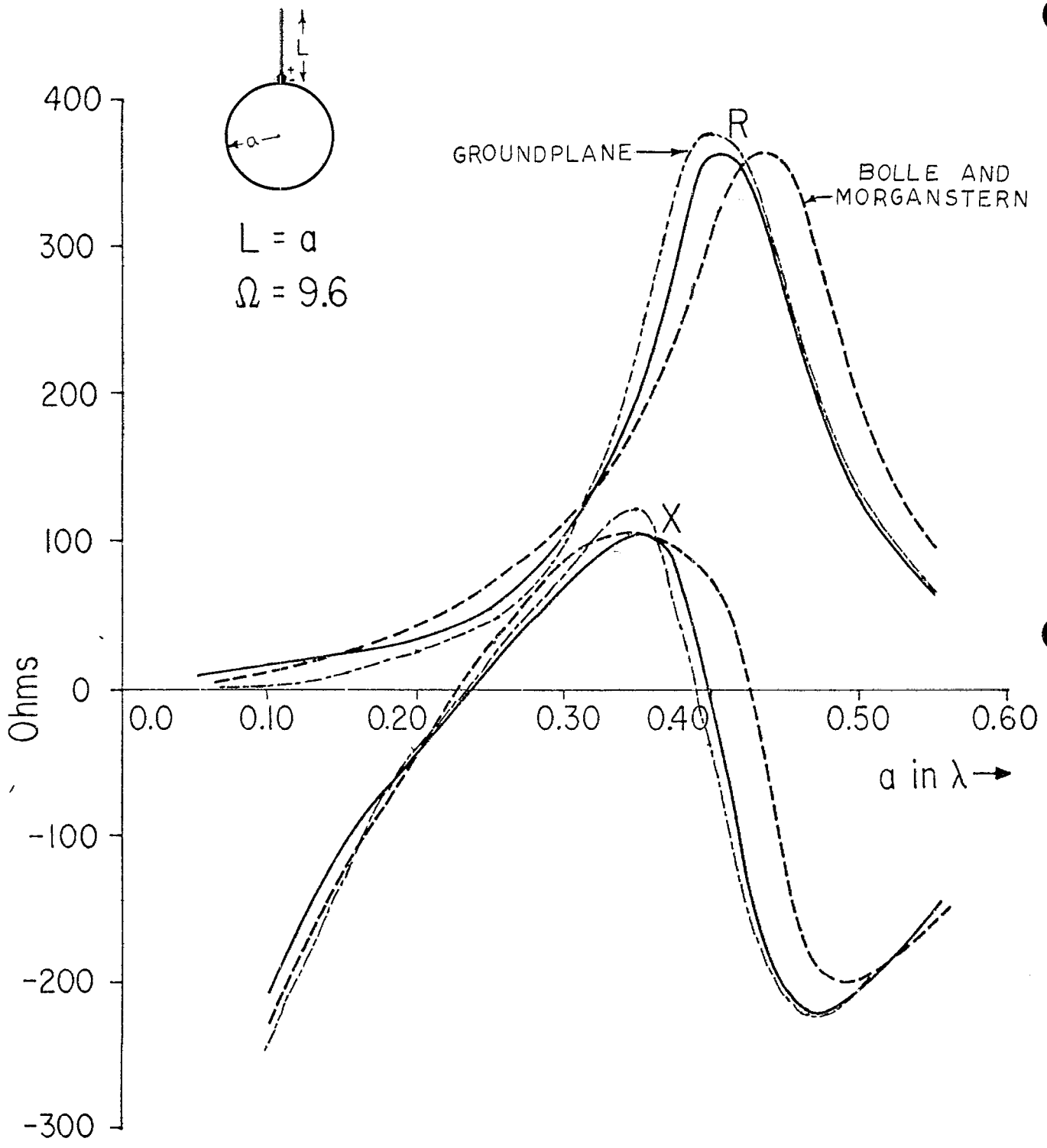

Figure 8. Input impedance of monopole on sphere (L = a) as a function of frequency (solid curves). Results for a perfect flat ground and those of Bolle and Morganstern are also indicated.

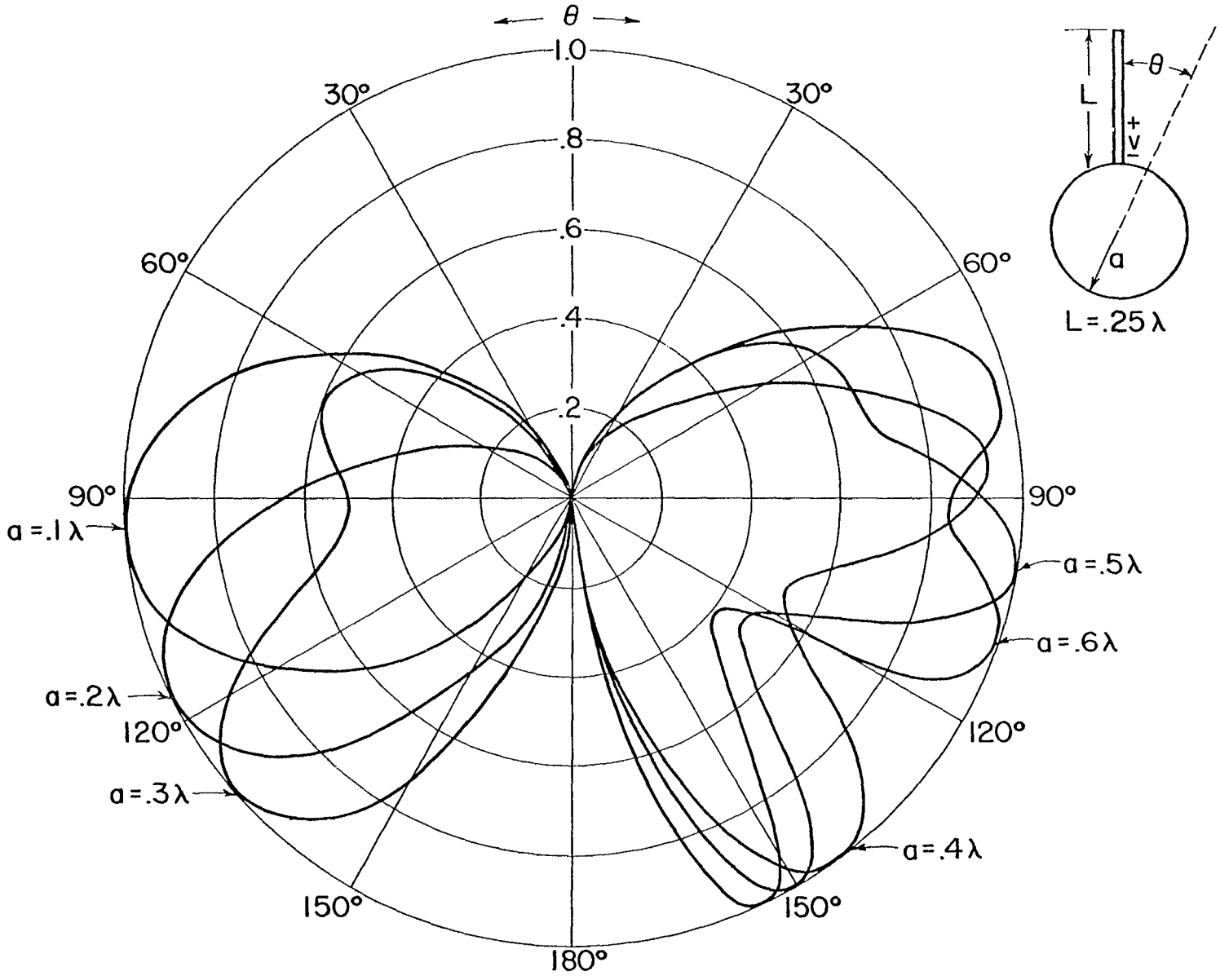

Figure 9. Radiation pattern for a single quarter wave monopole as a function of sphere radius.

that only half of the radiation pattern is presented due to the rotational symmetry involved. It is interesting to note that even though the input impedance of the monopole is relatively close to that of an infinite ground plane mount for $a = .5\lambda$, the radiation pattern is markedly different for each different value of a.

The total $\hat{\theta}$ directed current flowing on the sphere at any angle θ is shown in Figure 10 for three different sphere radii. This is obtained by evaluating the expression for the surface current density, J_θ, given in Eq. (34) and multiplying by $2\pi a \sin(\theta)$ to give the total current in the $\hat{\theta}$ direction. Note that the current values are for an assumed excitation of .5 volt at the antenna input. The real part of the current is negative at the input of the antenna at $\theta = 0$ due to the sign convention of the θ unit vector on the sphere.

With this general method of analysis, the mutual coupling between two or more antennas can be readily determined. As shown in Figure 11, the self and mutual admittances of two radial monopoles of lengths $L_1 = L_2$, $\Omega = 10$, mounted on the sphere are shown as a function of the angle between them. Two different sphere radii are considered. As an example of the application of these results to EMC analysis, it is noted that there is a minimum in the antenna coupling at $\theta \approx 138$ for a sphere size of $.5\lambda$. Thus, for minimum interference between the two antennas, their relative positions should be at that angle.

The total input admittance of the antennas previously discussed depends not only on the self and mutual admittances of the antennas, but on the excitation voltages of both antennas as

$$Y_{TOT} = Y_{11} + Y_{12}(V_2/V_1) \quad . \tag{36}$$

Thus, with the data presented in Figure 11, it is possible to obtain the total input admittance for an arbitrary source excitation. In Figure 12 the input admittance for the even ($V_1=V_2$) and odd ($V_1=-V_2$) modes of excitation are presented as a function of the angle θ. The sphere radius is $a = .25\lambda$. It is seen that the total input admittance depends to a great extent on the phasing of the exciting sources.

A symmetrical, four-arm spherical antenna as shown in Figure 13 has been analyzed also. For this structure, it was assumed that the monopole lengths were each $.25\lambda$ and had a shape factor of $\Omega = 10$. The

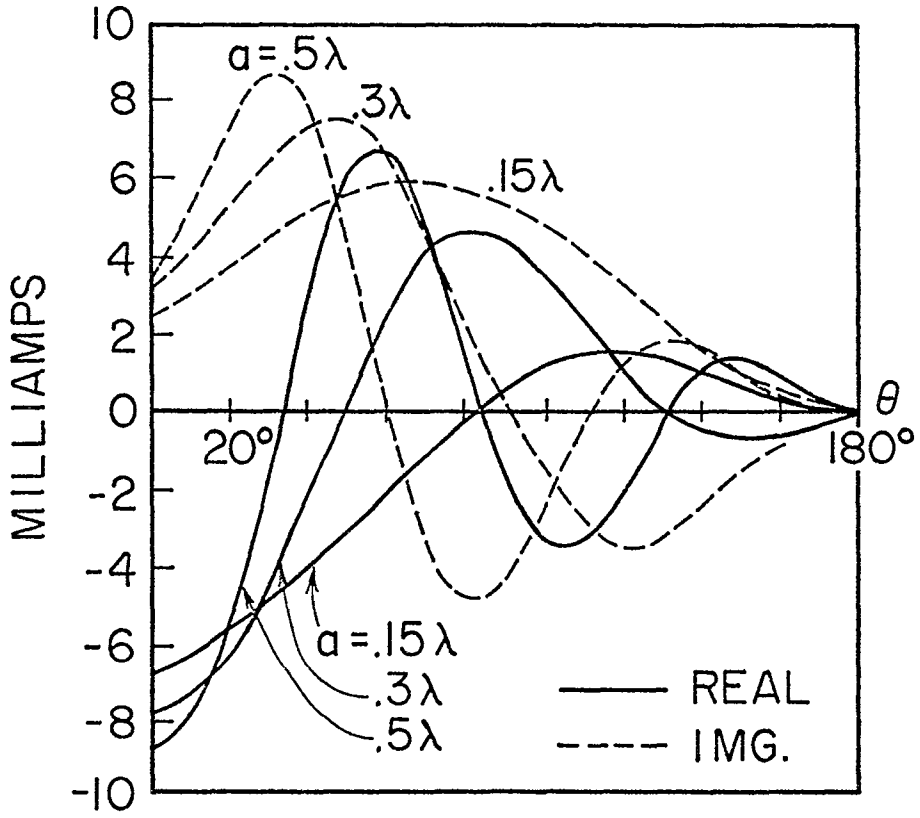

Figure 10. Total current flowing in the $\hat{\theta}$ direction on a sphere with an antenna of length .25L.

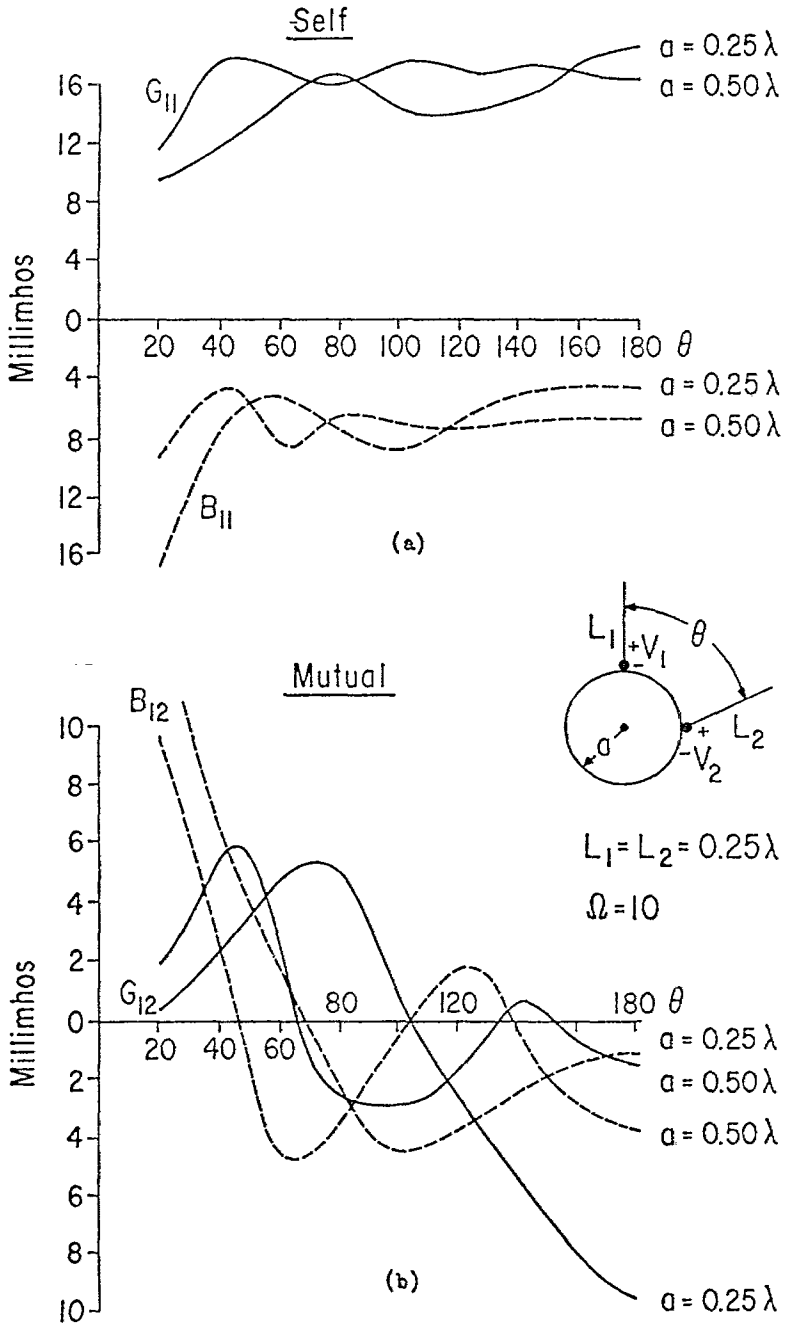

Figure 11. Self and mutual admittances of two quarter wave monopoles on sphere as a function at the angle θ.

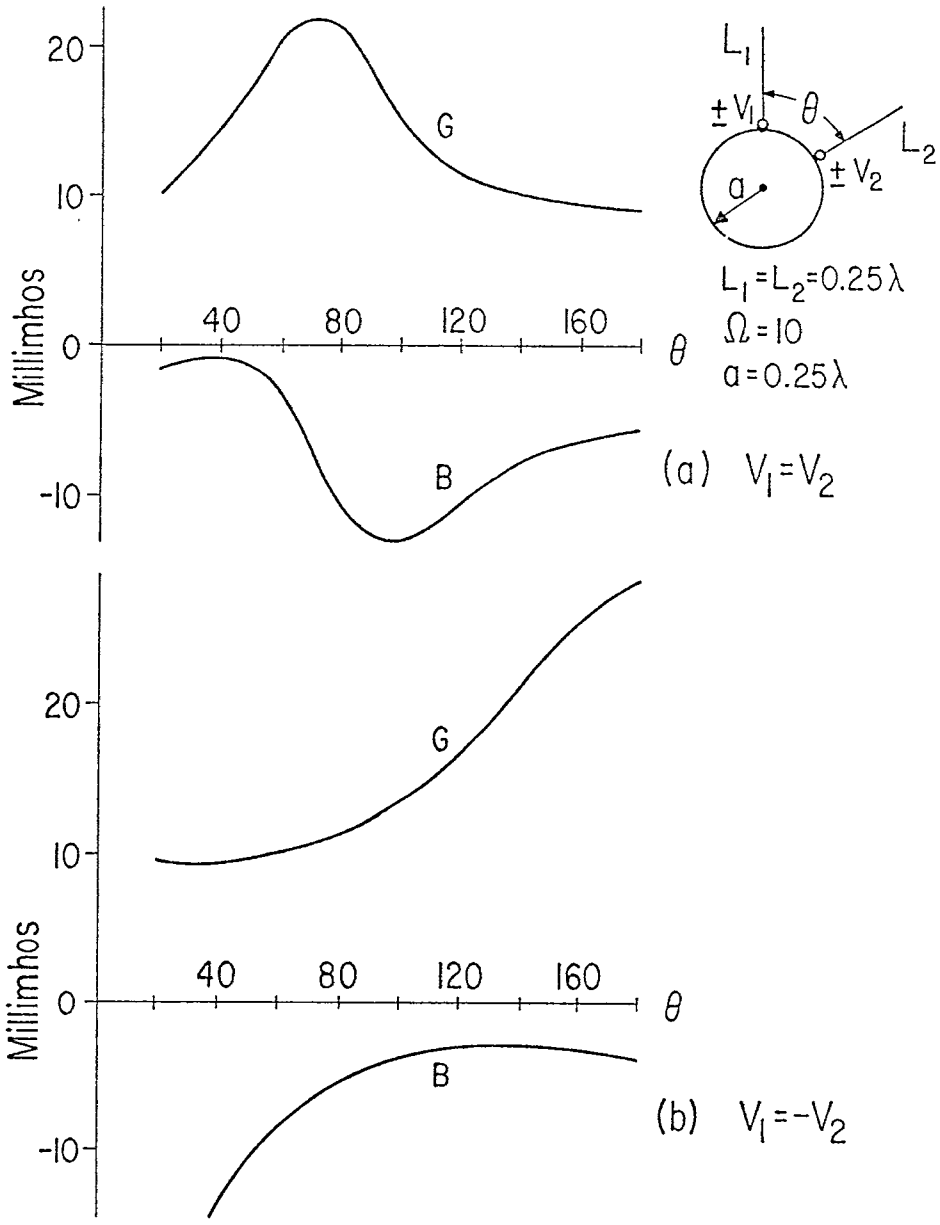

Figure 12. Total input admittance for two monopoles on a sphere of radius a = .25λ shown as a function of the angle θ. (a) is for even excitation and (b) is for the odd excitation.

driving voltages were each .5 volts. Figure 14 shows the total input admittance for each antenna, as well as the self and mutual impedances as a function of the sphere size. It is interesting to note that the real part of input current for the multi-arm antenna, when all antennas are driven in phase, is much smaller than that calculated on a single monopole on the same sphere, indicating a lower radiated power for each antenna. This can be related to the fact that a uniformly oscillating cloud of electrons does not radiate, and the multi-arm antenna has a much higher degree of symmetry than does the single monopole case.

The normalized magnitudes of the radiation fields $|E_\theta|$ and $|E_\phi|$ are shown in Figure 15 in polar form as a function of the polar angle θ for four different ϕ planes, $\theta = 0^\circ$, 10°, 20°, 30°. Because of symmetry, the pattern at $\phi = 40^\circ$ is identical to that of $\phi = 20^\circ$ and so forth. The normalized antenna gain $G(\theta,\phi)$ for this structure, defined as $G(\theta,\phi) = \sqrt{|E_\theta|^2 + |E_\phi|^2}$ is given in Figure 16. Du and Tai[3] have computed the radiated fields from point dipoles located on the same size sphere and at the same positions. As expected, the present results agree very well with their's, since the monopoles are still a fraction of a wavelength in length and behave much like point sources.

Figure 17 presents the current density J_θ and Figure 18 shows J_ϕ for the surface currents induced on the sphere for the four-arm symmetrical antenna.

Finally, the scattering problem is briefly treated in Figure 19. The delta-function spectrum of the short circuit current at the antenna input is shown along with the resulting step function excited transient behavior of the current. Notice the low frequency scalloping in the spectral response which is due to the resonances of the sphere.

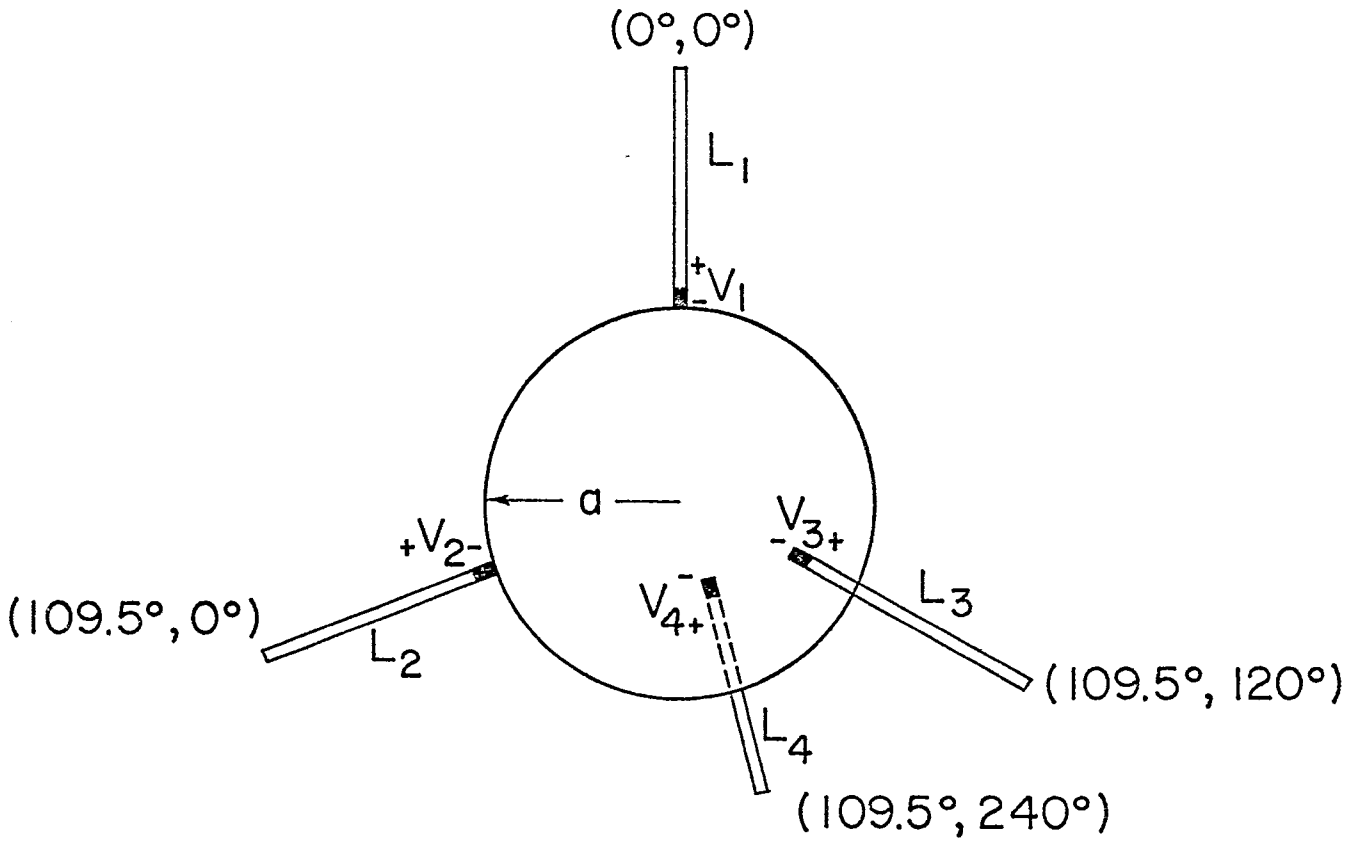

$$L_1 = L_2 = L_3 = L_4 = .25\lambda$$

$$V_1 = V_2 = V_3 = V_4 = .50\lambda$$

$$a = .50\lambda$$

$$\Omega = 10$$

Figure 13. Symmetrical, four-arm antenna.

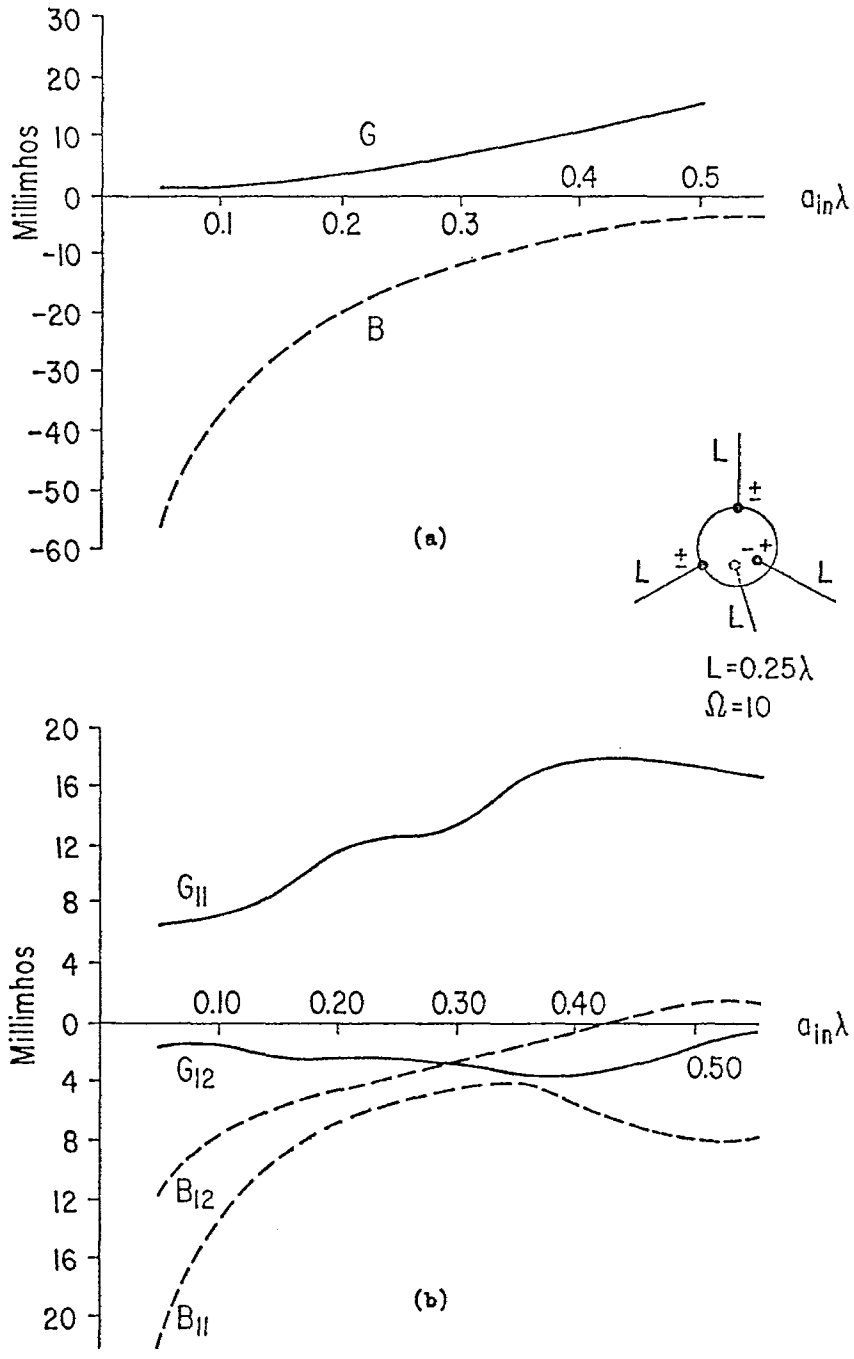

Figure 14. The input admittance (a) and the self and mutual admittances (b) for a symmetrical four-arm antenna as a function of the sphere radius.

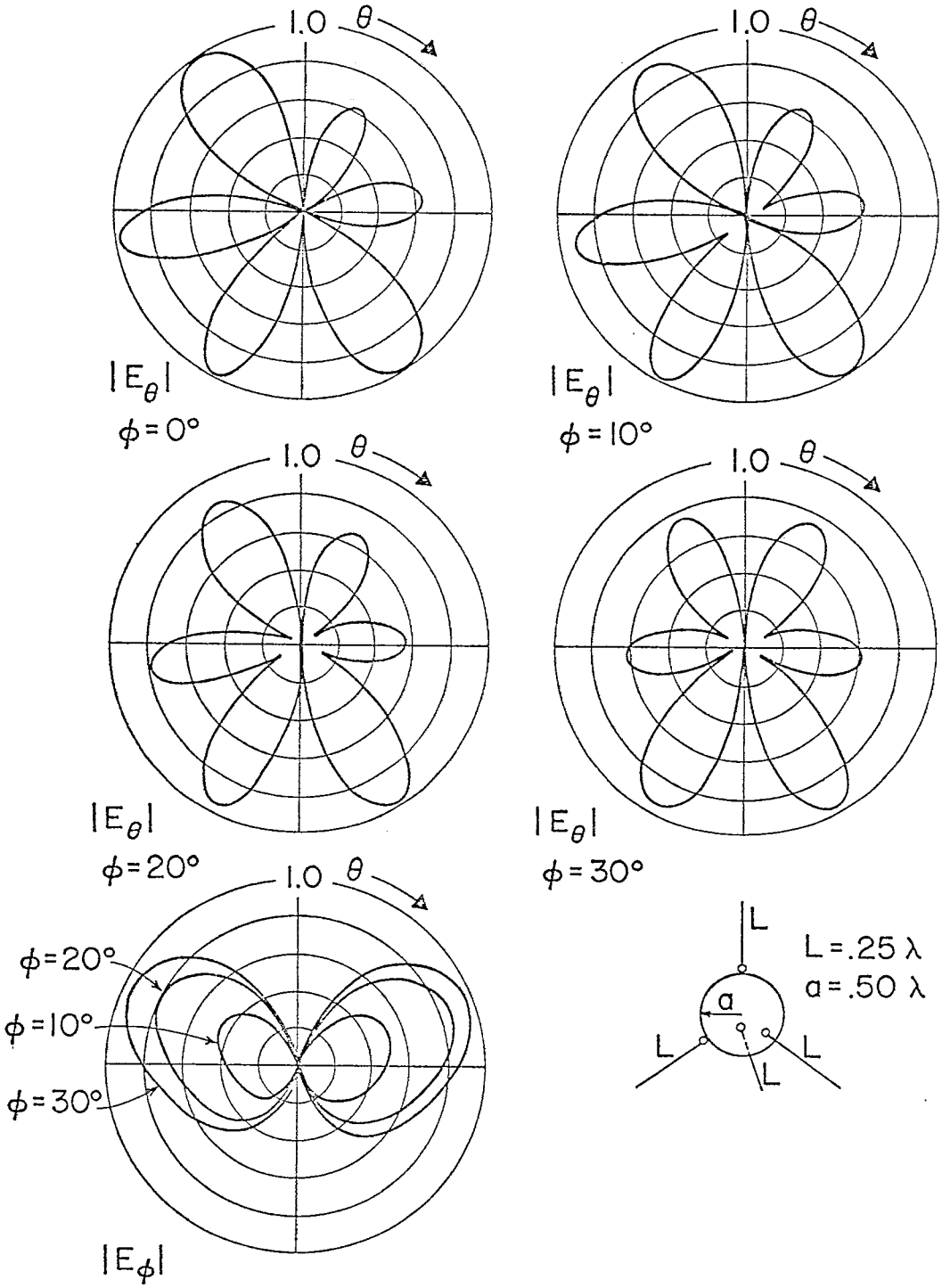

Figure 15. Normalized plots of $|E_\theta|$ and $|E_\theta|$ for the four-arm spherical antenna, with all arms driven in phase.

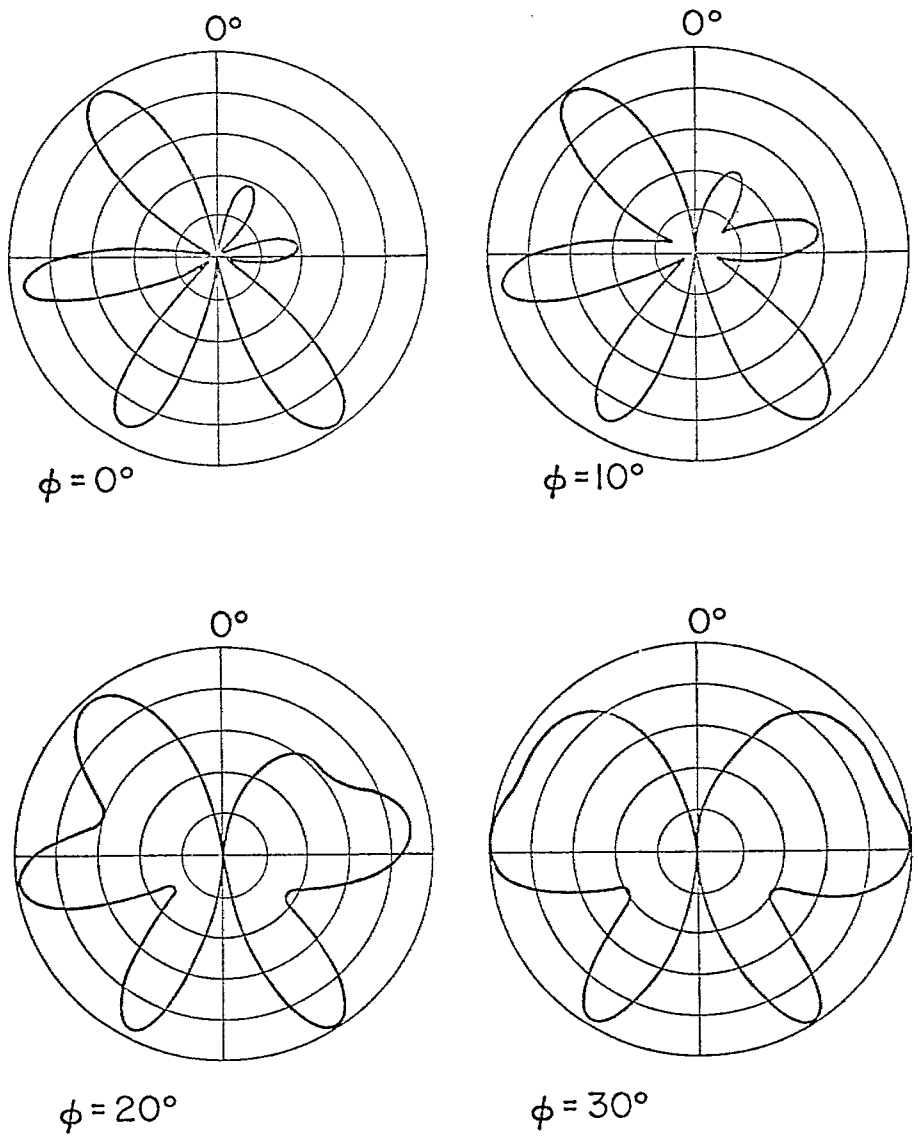

Figure 16. Normalized gain $G(\theta,\phi)$ for four-arm antenna.

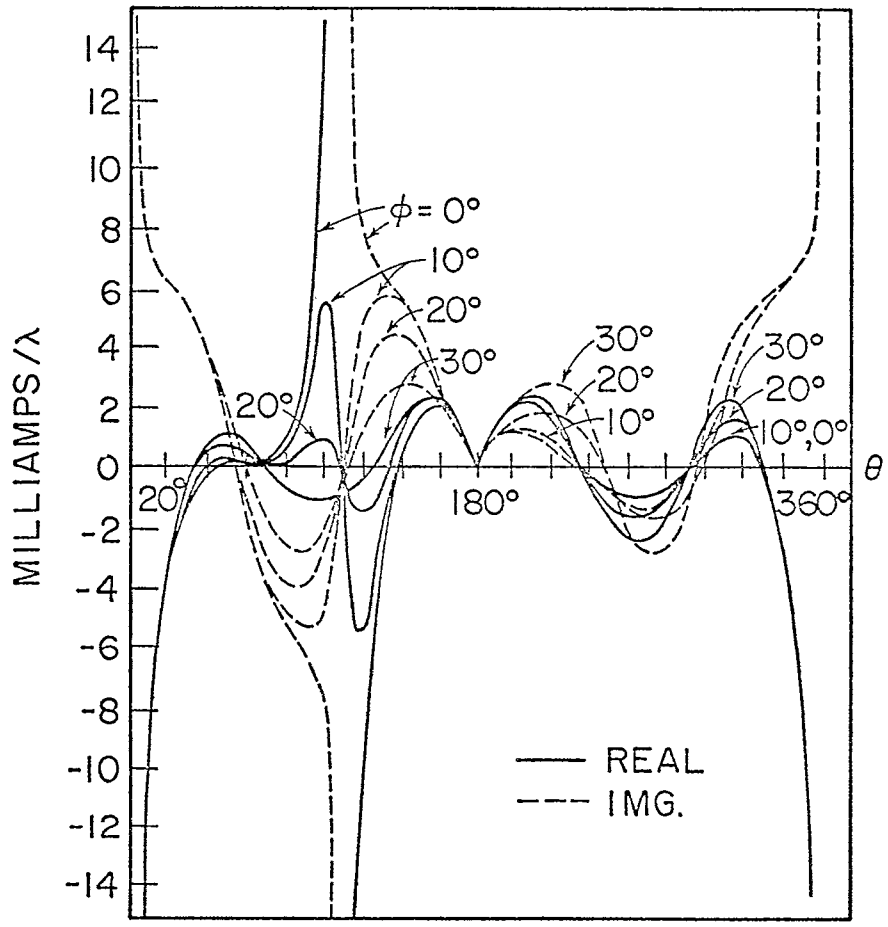

Figure 17. Current density on the sphere, J_θ, for the four-arm antenna L = .25λ, a = .5λ as a function of θ for various φ values.

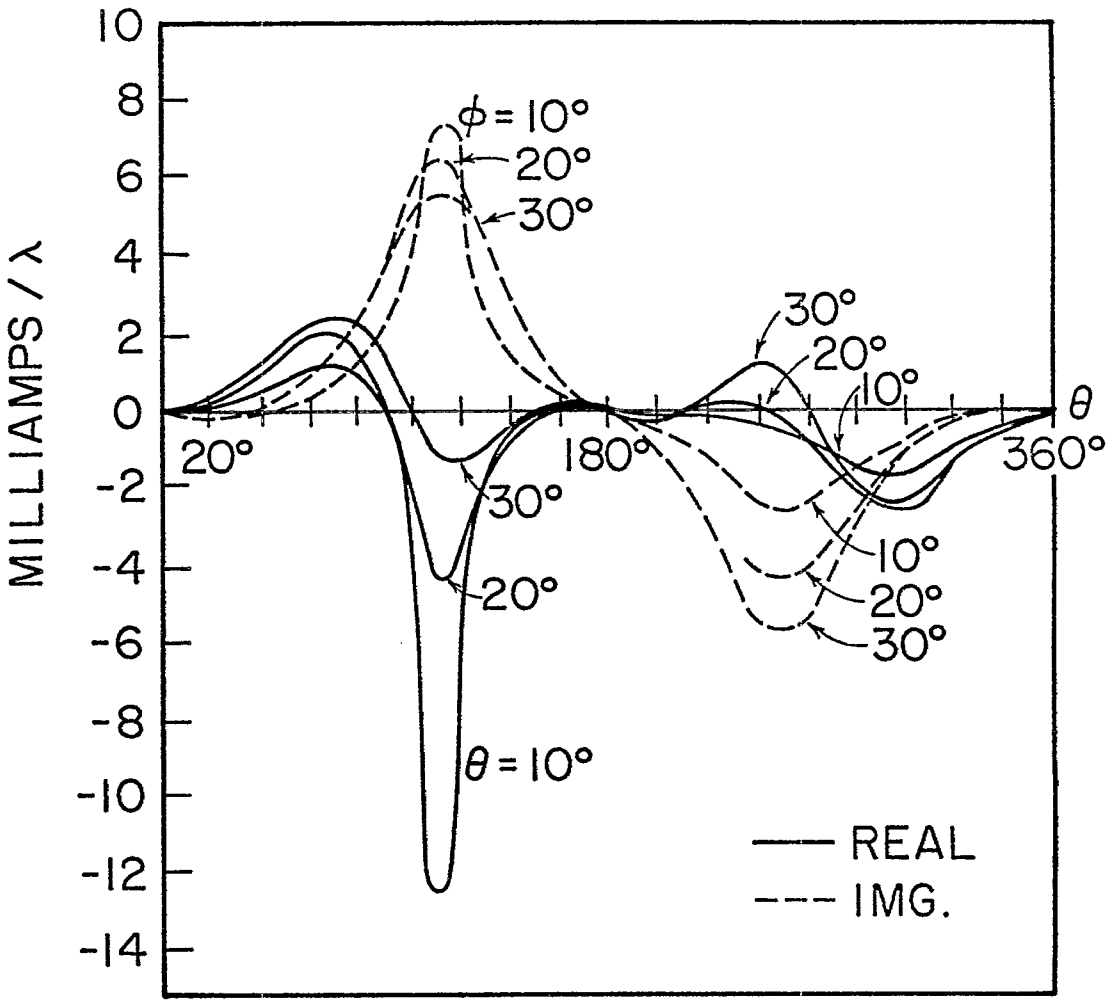

Figure 18. Current density on the sphere J_ϕ for the same four-arm antenna.

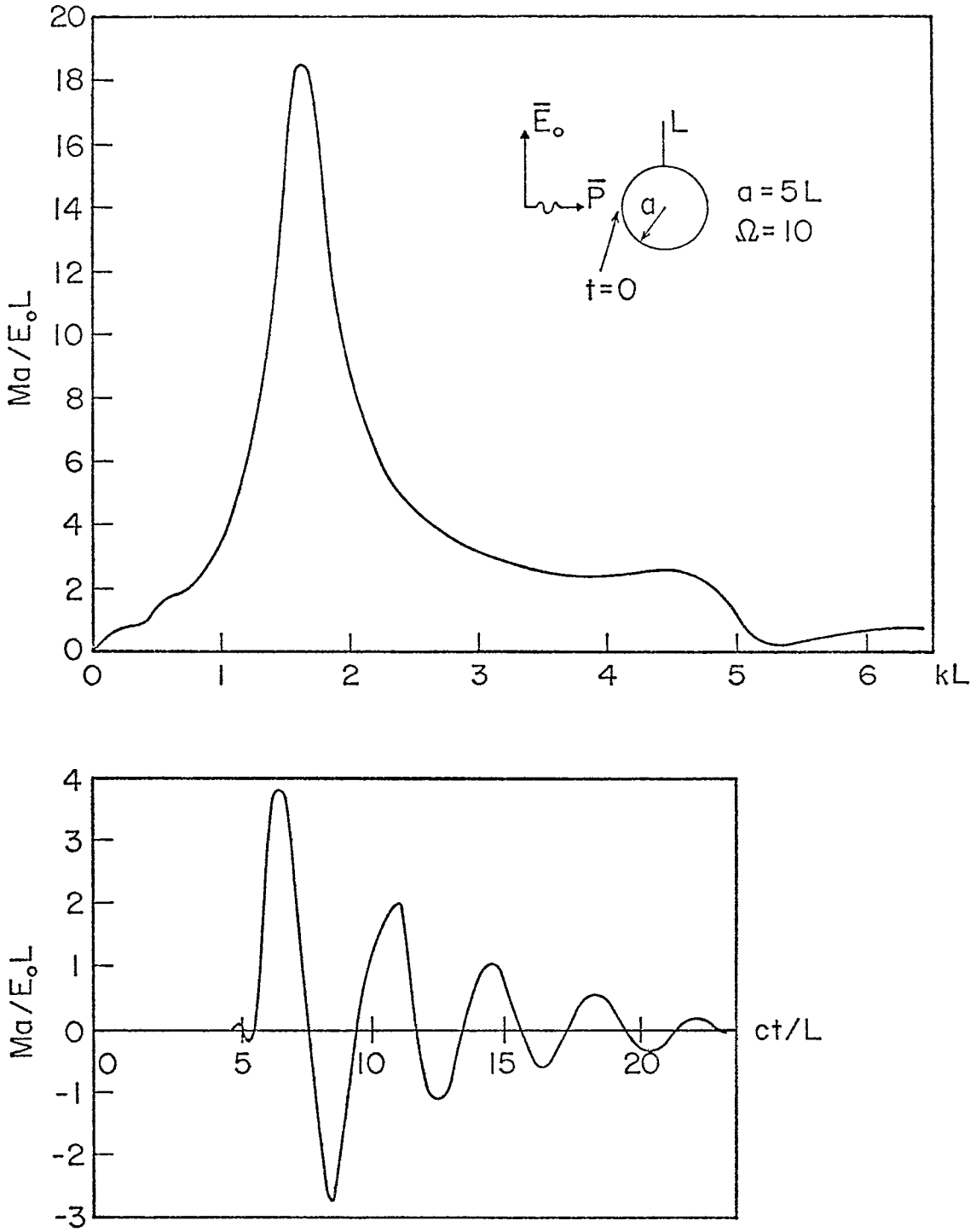

Figure 19. Induced current at the antenna input for scattering problem. a) Magnitude of δ-function frequency spectrum. b) Step function time response. The anomalous behavior at ct/L = 5 results from not using enough high frequency components in the spectrum.

VII. EXPERIMENTAL RESULTS

In an effort to determine the accuracy of the numerical methods, input impedance measurements were made for the two special cases shown in Figures 20a and 20b. When the monopoles are driven in phase, these two structures are easily analyzed using an image ground plane in conjunction with a network analyzer. The network analyzer is capable of providing swept frequency impedance information at any reference plane along a co-axial line. By driving the antenna with the co-axial line (as shown in Figure 21) and locating the reference plane at the base of the monopole, it is possible to obtain the input impedance of the structure over a wide range of frequencies.

The output of the network analyzer is in the form of amplitude and phase of the reflection coefficient, which is easily transformed into a complex impedance. By driving the Y-input of an X-Y recorder with the amplitude/phase output and driving the X-input with a frequency reference, a plot of the amplitude and phase of the reflection from the monopole as a function of frequency is obtained.

As King[12] has noted, the impedance loading the end of the co-axial line is not just the antenna impedance, but also includes effects due to the finite size of the aperture at the point of excitation. These fringing effects are not negligible, and they are particularly important at anti-resonance. These fringing effects can be modeled as a small negative capacitance, C_f, located at the end of the co-axial line.

In order to correct the theoretical results to account for the effects of the fringing capacitance, the method suggested by King[13] is employed. First, the case of a monopole over a ground plane is considered. Since the theoretical results are well known for the monopole[11], it is possible to add a small fringing capacitance to the source region so as to make the theoretical and measured anti-resonance occur at the same frequency. For the experimental setup employed, it was found that the fringing capacitance is -.076 pf.

It is now possible to investigate the two cases of interest. The fringing capacitance will change somewhat from that of the monopole over an image ground plane since the feed is located on a spherical

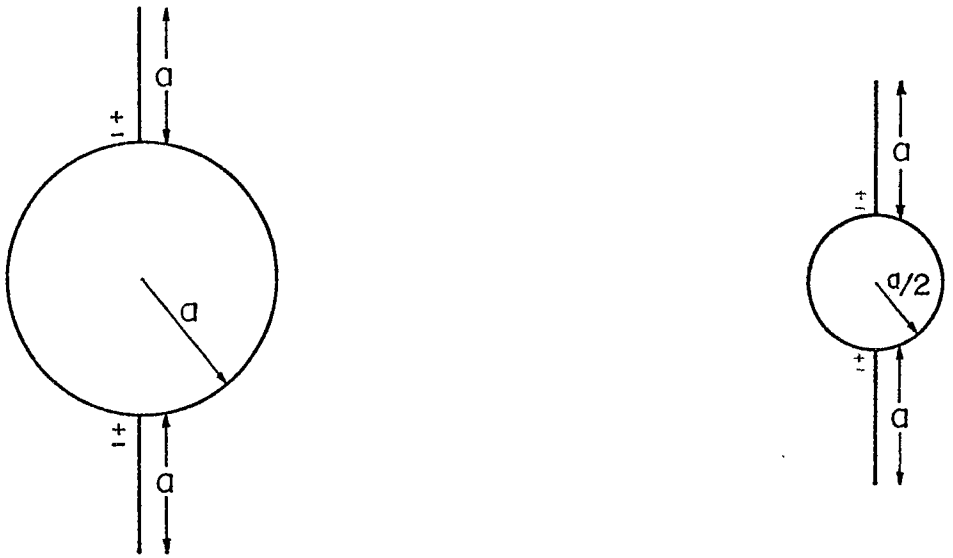

Figure 20. Geometries of structures examined experimentally. The value of the parameter a was 1 inch and the wire diameter was .035 inches.

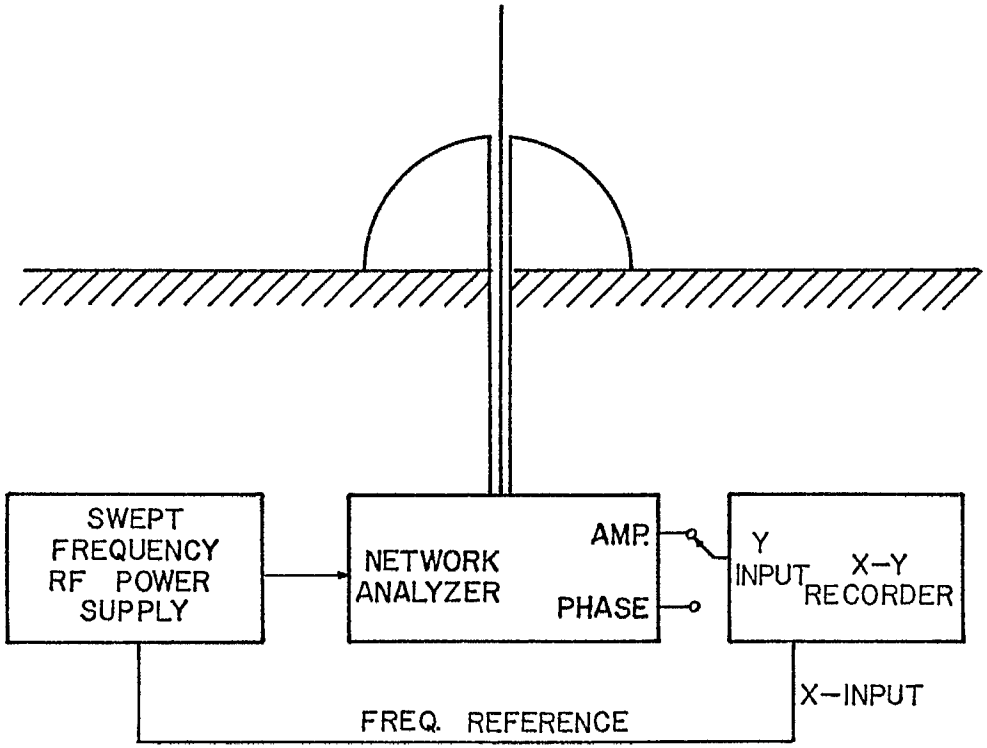

Figure 21. Test set-up.

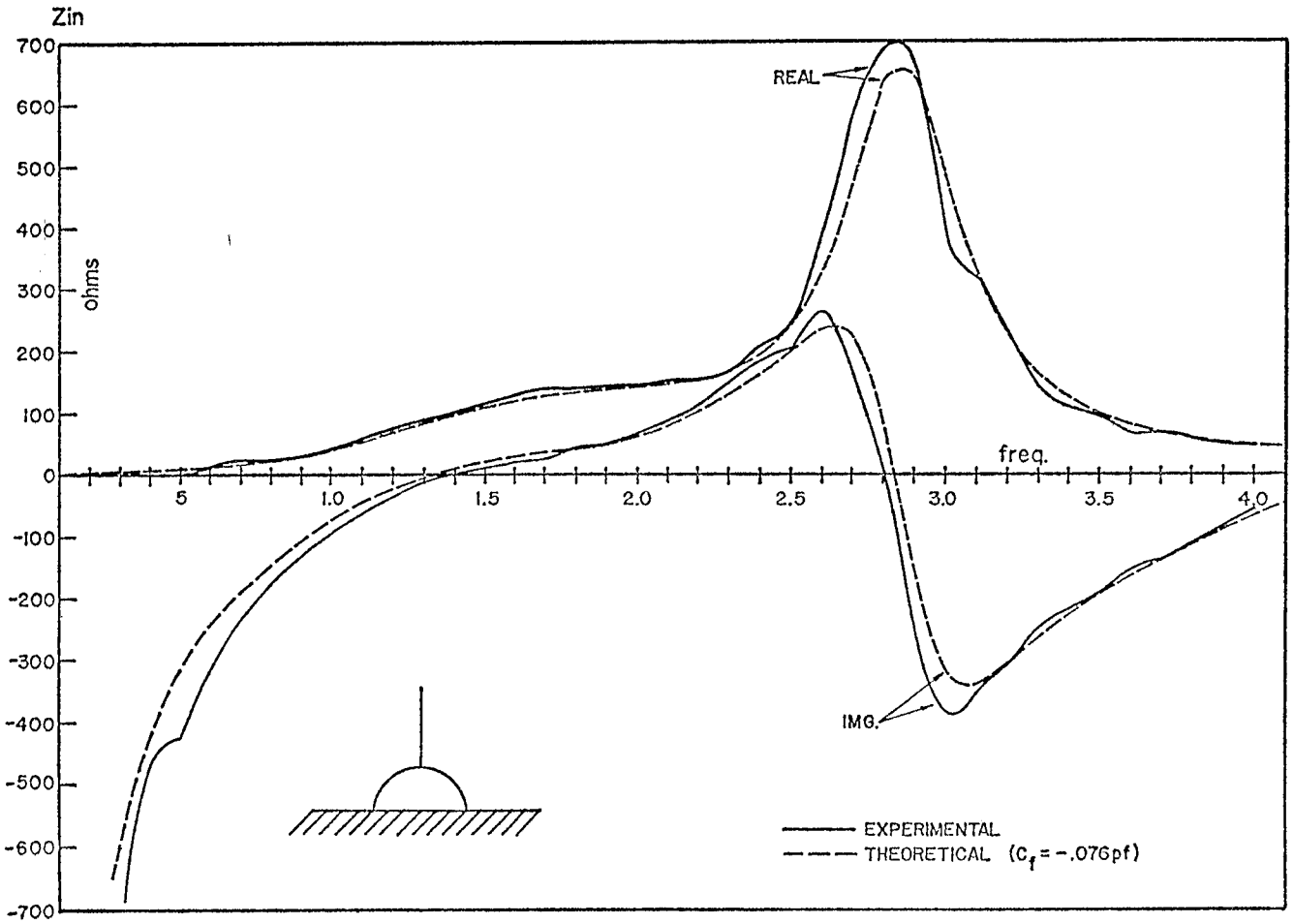

Figure 22. Theoretical and experimental values of input impedance as function of frequency (Gh) for L = 2 inches, a = 1 inch.

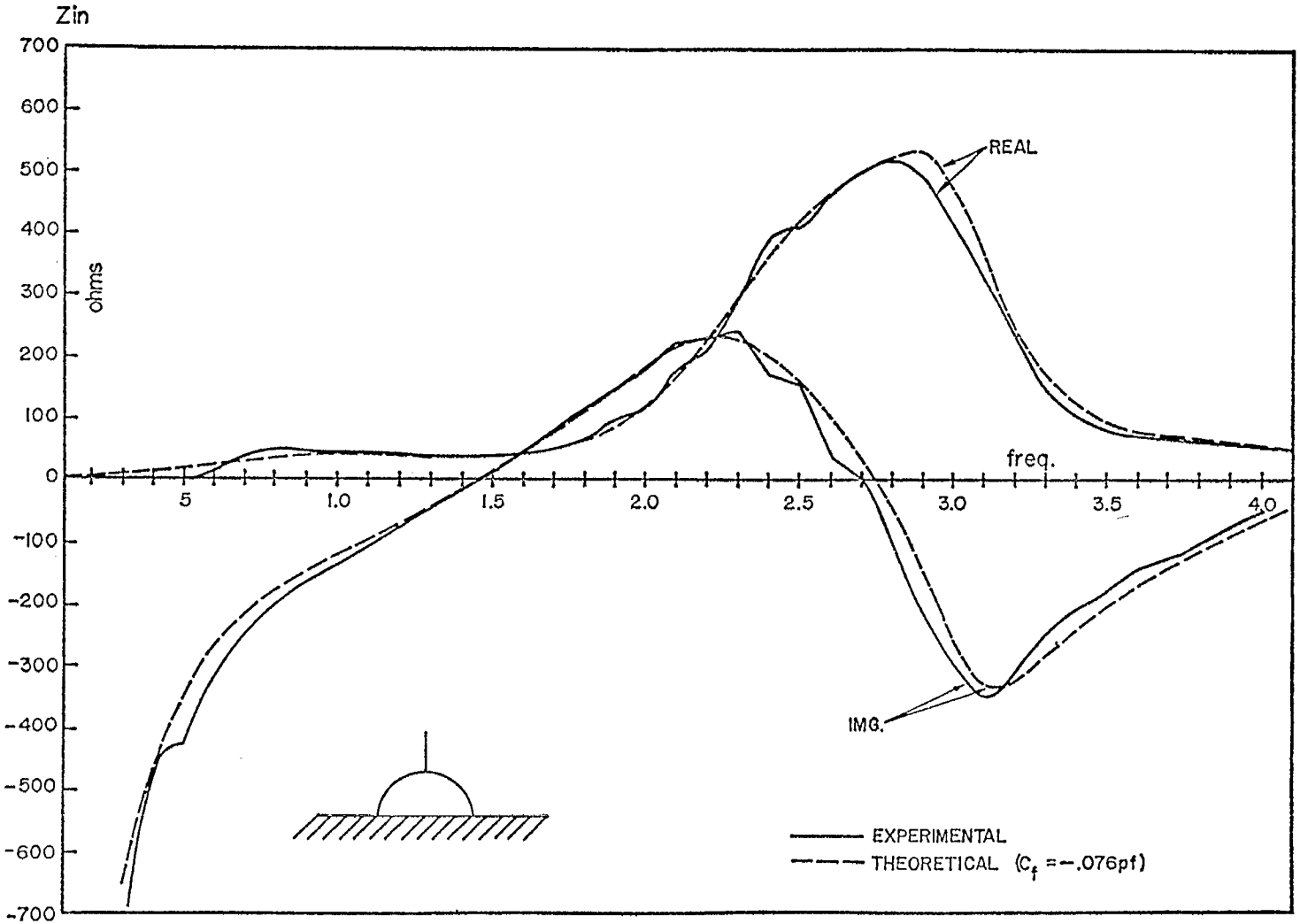

Figure 23. Theoretical and experimental values of input impedance as function of frequency (Gh) for L = 1 inch, a = 1 inch.

surface. To a good approximation, however, it is possible to assume the same fringing effects in these two cases. Figure 22 and Figure 23 show the theoretical and measured impedance (with and without a compensating C_f) and measured impedance as a function of frequency. The figures clearly show the excellent agreement between theoretical and experimental results.

VIII. CONCLUSIONS

In this paper, a technique for determining the behavior of thin-wire antennas located on a conducting sphere was discussed. This method consisted of formulating and then solving an integral equation for the antenna current, with the range of integration limited to over the wire only through the use of a modified Green's function. From the knowledge of the currents flowing on the wires, the input impedances, radiated fields, sphere currents and mutual coupling parameters can be easily computed.

The application of this method shows that it is numerically feasible in terms of computer time and storage requirements. Comparisons of the computed results with other data obtained through approximate analyses or other techniques show that this method is also accurate.

From the specific structures analyzed, a number of conclusions can be drawn about the spherical antenna.

1) The functional form of the current distribution on a radially directed monopole of length L mounted on the sphere is very close to that existing on the same monopole over an infinite ground plane. This implies that the form of the antenna current is relatively independent of the sphere size.

2) The input impedance of a monopole driven against the sphere depends upon the sphere radius, but for spheres of radius greater than $.5\lambda$, the input impedance is well within 8% of the impedance of the same monopole over an infinite ground plane.

3) The radiation patterns and the current distribution on the sphere are calculated through a rotational procedure. The most basic structure for these calculations is, therefore, that of one monopole along the polar axis of the sphere, since all other structures may be treated by rotating the coordinate system and adding the results.

4) For small spheres or other obstacles the radiation pattern is almost like that of the antenna of length L. As the obstacle size increases, its presence becomes important in determining the shape of the radiation pattern. The pattern for a single monopole of length $L = .25\lambda$ at the top pole of a sphere of radius "a" is similar to that of a quarter wave antenna for $a < .15$. As the sphere radius increases, the maximum in the radiation pattern begins to move away from the monopole location, resulting in a higher radiation intensity near the bottom of the sphere than near the top.

5) The current density on the sphere due to a single monopole at the pole of the sphere is seen to be oscillatory in nature. The total current on the sphere is zero at the opposite pole of the sphere as required by symmetry, and the magnitude of the current is seen to decrease as the observation point on the sphere surface moves away from the base of the monopole.

IX. REFERENCES

1. Abramowitz, M. and I.A. Stegun, Handbook of Mathematical Functions, National Bureau of Standards, Washington, D.C., 1968.
2. Bolle, D.M. and M.D. Morganstern, "Monopole and Conic Antennas on Spherical Vehicles", IEEE Trans. A.P., Vol. AP-17, July 1969, 477-484.
3. Du. L. and C.T. Tai, "Radiation Patterns for Symmetrically Located Sources on a Perfectly Conducting Sphere", Ohio State University Research Foundation Report 169-10, Dec. 15, 1964.
4. Harrington, R.F., Field Computation by Moment Methods, MacMillan, New York, 1962.
5. Harrington, R.F. and J.R. Mautz, "Computation of Green's Functions for Bodies of Revolution", Interaction Note 190, July 1970.
6. Harrington, R.F., Time Harmonic Electromagnetic Fields, McGraw-Hill, New York, 1961.
7. Jackson, J.D., Classical Electrodynamics, Wiley, New York, 1962.
8. Jones, D.S., The Theory of Electromagnetism, Pergamon Press, London, 1964.
9. Kalhor, H.A., "Study of Scattering of Electromagnetic Waves by Periodic Structures with Sharp Edges", Ph.D. dissertation at University of California, Berkeley, September 1970.
10. Kammler, D.W., "Numerical Solution of the Dirichlet Problem for Systems of Circular Conductors Between Parallel Ground Lines", Math. Comp. 213, June 1969, 29-36.
11. King, D.D., "Measured Impedance of Cylindrical Dipoles", Journal of App. Phys., Vol. 17, 1946, 844.
12. King, R.W.P., Transmission Line Theory, McGraw-Hill, New York, 1955.
13. King, R.W.P., Theory of Linear Antennas, Harvard Press, Cambridge, 1956.
14. Rao, B.R., "Current Distribution and Impedance of an Antenna in a Parallel Plate Region", Proc. IEE (London), Vol. 112, Feb. 1965, 259-268.
15. Scherer, J.P. and A.R. Neureuther, "Mutual Coupling in Linear Dipole Arrays", IEEE Trans. A.P., Sept. 1972, 651-653.

16. Shanks, D., "Nonlinear Transformations of Divergent and Slowly Converging Sequences", Journal of Mathematics and Physics, XXXIV, 1955, 1-42.

17. Tai, C.T., Dyadic Green's Functions in Electromagnetic Theory, Intext Publishers, 1971.

18. Taylor, C.D., and G.A. Steigerwald, "On the Pulse Excitation of a Cylinder in a Parallel Plate Waveguide", Sensor and Simulation Note 99, March 1970. See also IEEE Trans. A.P., Vol. AP-51, July 1967, 572-574.

19. Tesche, F.M. and A.R. Neureuther, "Radiation Patterns for Two Monopoles on a Perfectly Conducting Sphere", IEEE Trans. A.P., Vol. AP-18, No. 5, Sept. 1970, 692-694.

20. Tesche, F.M., "On the Behavior of Thin-Wire Scatterers and Antennas Arbitrarily Located within a Parallel Plate Region I. (The Formulation)", Interaction Note 75, May 1971. See also IEEE Trans. A.P., Vol. AP-20, July 1972, 482-486.

21. Tesche, F.M., "The Effect of the Thin-Wire Approximation and the Source Gap Model on the High-Frequency Integral Equation Solution of Radiating Antennas", IEEE Trans. A.P., March 1972, 210-211. See also Appendix 1 of Sensor and Simulation Note 141, Feb. 1972.

22. Tesche, F.M., "On the Analysis of Scattering and Antenna Problems Using the Singularity Expansion Technique", IEEE Trans. A.P., Vol. AP-21, No. 1, Jan. 1973, 53-62. See also Interaction Note 102, April 1972.

23. Watson, G.N., "The Diffraction of Electric Waves by the Earth", Procs. of the Royal Society, Vol. 95, 1919, 83-99.